PROTON AND HELIUM NUCLEI COSMIC RAY SPECTRA AND MODULATIONS BETWEEN 100 AND 2000 MEV/NUCLEON

by

Jonathan F. Ormes

Technical Report
CR-109

December, 1967

School of Physics and Astronomy
University of Minnesota
Minneapolis, Minnesota

*Research supported by NASA Support Grant NsG 281-62.
A Thesis submitted to the faculty of the Graduate School of the University of Minnesota in partial fulfillment of the requirements for the Degree of Doctor of Philosophy, December, 1967

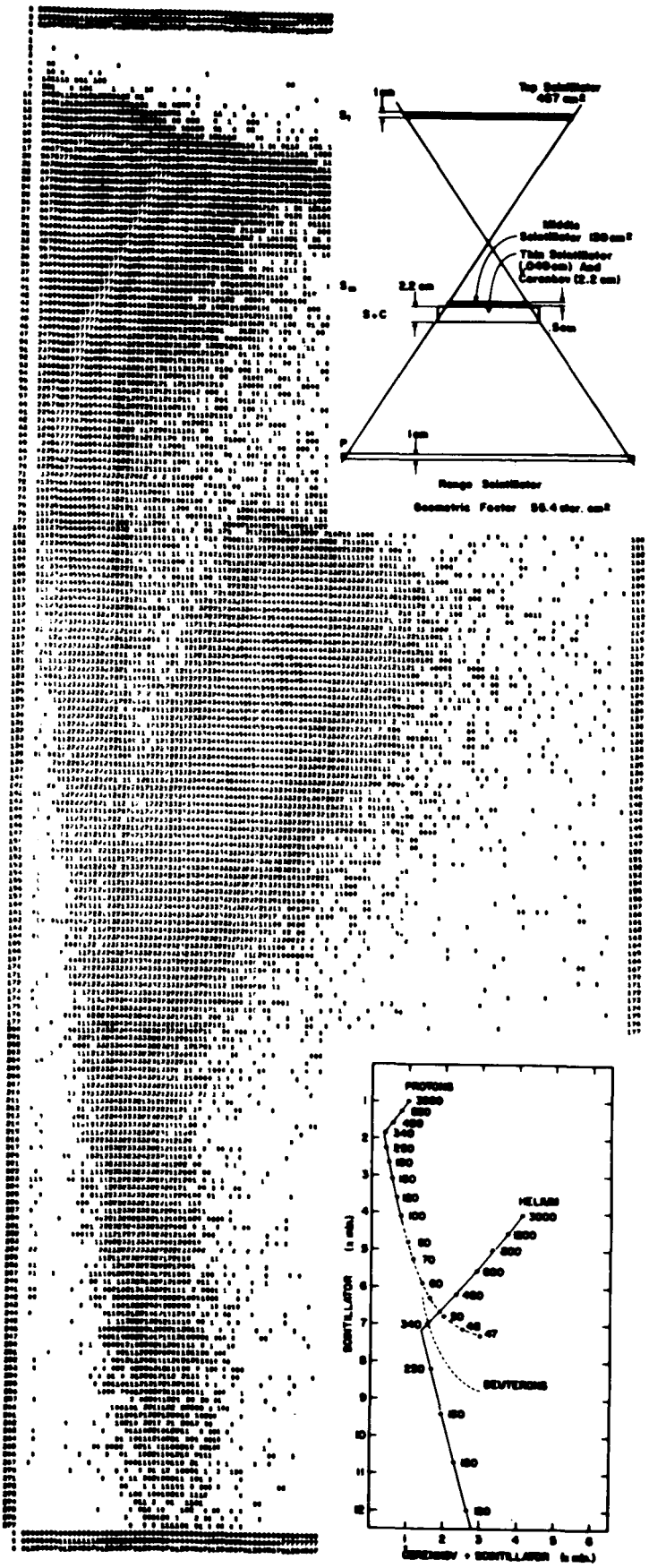
Top Scintillator
407 cm²
1cm
S1
Middle
Scintillator (50 cm²
Thin Scintillator
(.040cm) And
Carnbon (2.2 cm)
S2
2.2 cm
S.C
5cm
P
1cm
Range Scintillator
Geometric Factor 56.4 ster. cm²
PROTONS
HELIUM
DEUTERONS
SCINTILLATOR (1 mils)
(CERENKOV + SCINTILLATOR (1 mils)

ACKNOWLEDGEMENTS

I should like to express my deepest appreciation to Dr. W.R. Webber who has directed this research and provided guidance and encouragement throughout. His generosity with his time and his ideas has been of enormous value in this research.

I would next like to thank Dr. C.J. Waddington and Dr. P.S. Freier for their interest in this work and their helpful criticism.

For the many flights we have had with this equipment and for their help in the analysis of the data I am indebted to Mr. John Graham, Mr. James Kish and Mr. Donald Kvist.

The typing has been done by Mrs. Grace Pauls and I am most grateful to her, especially for being able to read my writing.

I appreciate the hospitality of the Great Western Hotel in Hughenden, Queensland, Australia, where this paper was finally completed.

My gratitude to my wife for her patience has been duly communicated.

This work has been supported by the National Aeronautics and Space Administration Grant NsG 281-62.

ABSTRACT

During the years 1963-1966, as the sun passed through its minimum period of activity, an extensive series of balloon flights has been conducted in order to study the primary cosmic radiation and its time variations. The instrument used is a Cerenkov-scintillation counter telescope, the most recent version of which contains two dE/dX detectors, a combination Cerenkov and scintillation detector and a range scintillator. This telescope and its response characteristics to protons and helium nuclei are described.

Convolution techniques are used to unfold the Landau fluctuations in energy loss thereby allowing derivation of the differential energy spectrum from 100 MeV/nucleon up to 2 BeV/nucleon.

The differential energy spectra derived by this technique are presented from nine balloon flights, five at Fort Churchill, Canada and four at latitudes ranging from Ely, Minnesota to Fayetteville, Arkansas. The spectra thus derived are found to be in generally good agreement with those of other workers but significantly more accurate. The spectra at lower latitudes clearly show the effects of the geomagnetic cut-off.

The data is examined to determine the functional form of the solar modulation by comparing the sunspot minimum spectrum obtained in 1965 with the pre-sunspot minimum spectrum obtained in 1963 and the post sunspot minimum spectrum obtained in 1966.

The modulation data does not follow a functional form of either $1/\beta$ or $1/\beta R$ but rather a form more nearly like $1/\beta R^{\frac{1}{2}}$. A theoretical picture is considered in which this behavior can be ascribed to the statistical distribution of magnetic scattering center sizes in the interplanetary medium. In this model the exponent of the rigidity dependent term in the modulation can be related to the slope of the power spectrum of magnetic scattering centers.

The data is compared with that of other workers and found to be consistent with a picture in which the form of the modulation above 200 MeV/nucleon changes from $1/\beta R^{\frac{1}{2}}$ near sunspot minimum to almost $1/\beta R$ near sunspot maximum. It is also observed that, at all levels of solar modulation, there is a rigidity below which the form of the modulation becomes $\simeq 1/\beta$. The rigidity below which the form $1/\beta$ holds varies systematically during the solar cycle, but differently for protons and helium nuclei in a manner which is difficult to understand within the framework of the current solar wind models for the modulation.

TABLE OF CONTENTS

LIST OF FIGURES

I. INTRODUCTION

It has been known for some time that the intensity of cosmic rays near the earth is inversely correlated with the 11 year cyclic activity on the solar surface as expressed through the number of sunspots. Models which connect this modulation of cosmic rays (called the long term modulation) with the solar activity have ranged from the heliocentric electric fields envisaged by Emhert (1960) and the solar dipole magnetic field of Elliot (1960) to the more generally accepted solar wind model first developed by Parker (1956).

In this latter model the connection between solar activity and the cosmic ray modulation was proposed to be made through the expanding corona of the sun (the solar wind). The feature of the solar wind which is supposedly responsible for the cosmic ray variation near the earth is the "frozen in" magnetic field which is carried away from the sun by this plasma. This magnetic field and, in particular, its inhomogeneities are imagined to sweep the cosmic rays out of the solar system thus producing intensity variations. With the advent in recent years of satellites which have gone outside the earth's magnetosphere, the existence of the solar wind and the interplanetary magnetic field has been verified.

Parker's original model has been modified and expanded by many authors. It suffices to say that each modification of the model makes specific predictions regarding the rigidity

dependence of the modulation. It is the purpose of this paper to examine that functional form (e.g. rigidity dependence) experimentally.

In this connection many attempts have been made during the last four years, 1963-1966, while the sun has gone through its period of minimum activity, to determine the functional form of the modulation. These attempts have not been sufficiently accurate nor have they extended over a sufficiently large energy range to enable the important parameters of this model to be investigated, to study its limitations, or to search for other less important processes which may be at work. In an attempt to remedy this situation we have designed and flown a large area Cerenkov scintillation counter telescope to study the variations of both the proton and helium components.

This series of Cerenkov scintillator measurements began in 1963 and is still continuing. During this time the balloon borne particle detection system has evolved considerably and the most recent version of the telescope and the details of its response will be described here.

In order to extend the measurements of the differential energy spectrum over the whole range from 100 MeV/nucleon up to 2 BeV/nucleon, a new method for the derivation of the energy spectrum from a pulse height distribution has been developed and will be presented. In addition we will deal specifically with the problems of background, statistical energy loss fluctuations, energy calibration and atmospheric secondary corrections as they pertain to the derivation of

the energy spectra.

We will then present the differential energy spectra of both protons and helium nuclei obtained on nine balloon flights, five at Fort Churchill, Manitoba and four at lower latitudes ranging from Fayetteville, Arkansas to Ely, Minnesota.

These spectra will be examined to determine the functional form of the solar modulation. It will be shown that at solar minimum in the energy range covered by this detector the modulation is neither of the two most commonly assumed forms, $1/\beta$ or $1/\beta R$, but lies somewhere between -- say $1/\beta R^{\alpha}$ where α is .5 or .6. Other data available on the 11 year modulation will be examined in view of this finding.

Before proceeding, a final introductory remark is in order. The large energy range accessible to this detector makes it possible to eliminate some of the difficulties encountered in studies which depend upon summaries of the data from several detectors over several different energy ranges (e.g. see Silberberg, 1966, or Nagashima et al., 1967). The advantage of using a single detector, and very importantly, a single method of analysis over a large energy range is clearly to systematize the errors which can always be present in the data analysis of any counter experiment. For this reason it is hoped that measurements can continue to be made with this detector throughout the remainder of the current solar cycle.

II. THE DETECTOR

The measurements to be considered here have been selected from twelve successful balloon flights made during the years 1963-1966 at a number of locations, but primarily at Fort Churchill, Manitoba.* During this period the cosmic ray intensity reached a maximum during the early part of 1965. The details pertinent to the balloon flights are given in Table 1 along with the corresponding neutron monitor intensities from Mt. Washington. The measurements are seen to range from within 6% to 2% of sunspot minimum conditions as determined from the highest Mt. Washington neutron monitor rates reached in 1954-1955 and again in 1965.

A detailed description of the experiment can be found in a University of Minnesota Technical Report (Ormes, 1965). This discussion includes a description of the physics, the resolution, the electronics, the calibration, the non-linearities, the stability, etc. of the telescope and information concerning the data analysis and the logistical balloon support. Here we will be concerned only with those features which relate directly to the validity of the data to be presented.

Figure 1 is a schematic diagram of the most recent version

---

*Preliminary proton and helium spectral data has been presented elsewhere (Webber and Ormes, 1963 b; Ormes and Webber, 1964 and 1965), and results concerning other features of the data such as spectra of heavy nuclei, solar neutrons, and the He_3 and He_4 ratio have been reported (Webber and Ormes, 1963 a and 1965; Webber, Ormes and von Rosenvinge 1965; and Ormes, von Rosenvinge and Webber, 1967).

Table 1

Flight	Date	Mt. Washington neutron monitor day	Mt. Washington neutron monitor flight	Floating Depth (including gondola) gm/cm^2	Collection time (sec)	Geometrical Collection Factor*
Minneapolis	July 4, 1963	2318	2329	7.9	7079	32.9/36.5
Churchill 63	July 29, 1963	2292	2295	5.4	2865	32.9/36.5
Devils Lake	Nov. 11, 1963	2313	2314	8.1	12791	32.9/36.5
Fayetteville	Mar. 29, 1964	2366	2378	6.6	17505	37.2/41.1
Ely	May 23, 1964	2412	2418	6.0	17810	37.2/41.1
Churchill 65-1	June 23, 1965	2436	2444	4.3	18213	44.9
Churchill 65-2	July 11, 1965	2426	2423	2.6	23601	37.2/41.1
Churchill 66-1	July 13, 1966	2337	2355	3.7	28764	55.4
Churchill 66-2	July 25, 1966	2367	2365	3.3	35418	55.4

*Geometrical Factor increases at 320 MeV/nucleon in the original version of detector.

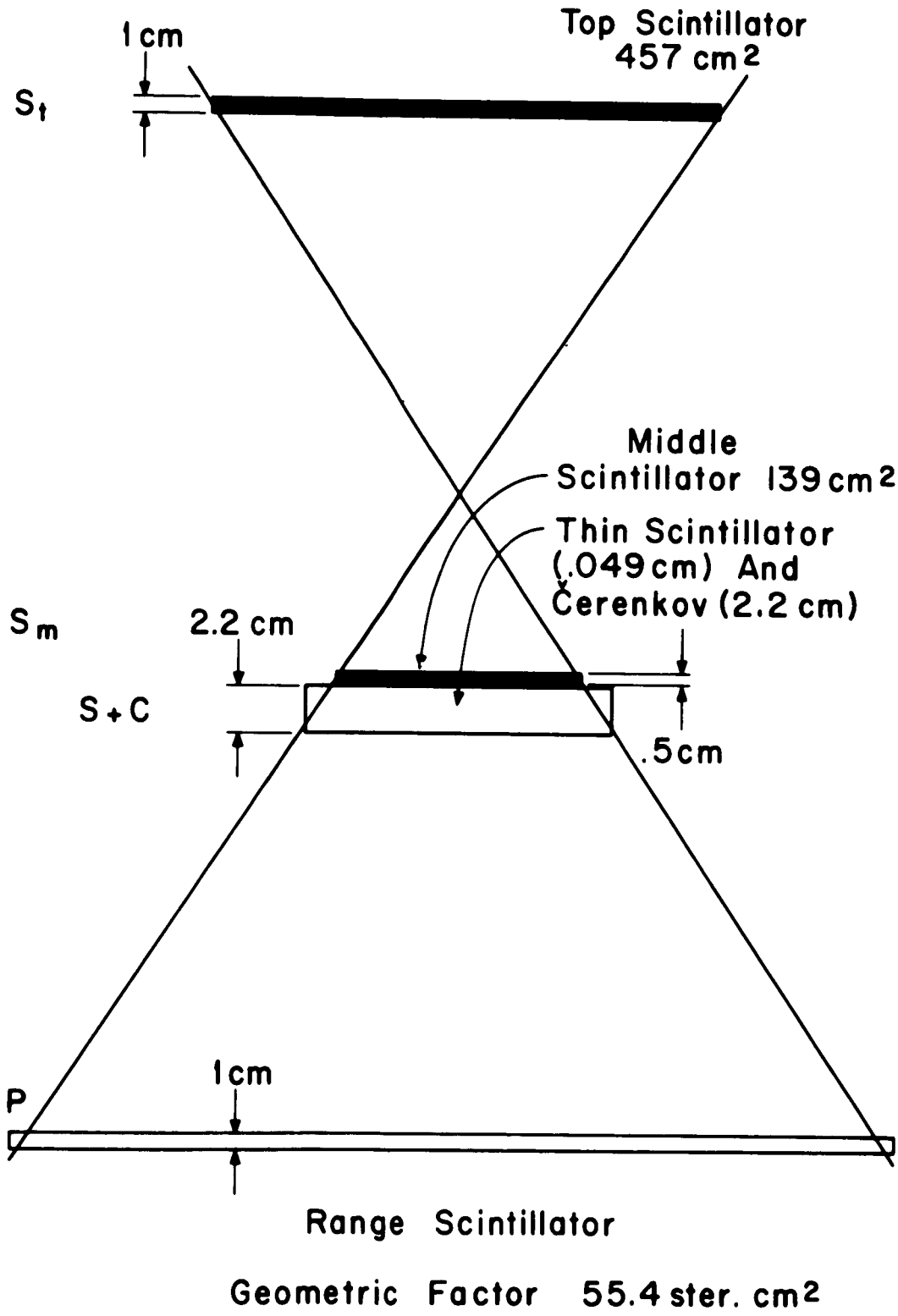
1 cm
Top Scintillator
457 cm2
St
Middle
Scintillator 139 cm2
Thin Scintillator
(.049 cm) And
Cerenkov (2.2 cm)
Sm
2.2 cm
S+C
.5 cm
1 cm
P
Range Scintillator
Geometric Factor 55.4 ster. cm2

Figure 1

of the counter telescope. A coincidence event is defined by the first two elements, (S_t and S_m), both NE (Nuclear Enterprises) 102 plastic scintillator. The ionization loss in both of these detectors results in light pulses which are analyzed and recorded by a 2048 channel pulse height analysis system. The third element is a combination scintillator and Cerenkov detector called the S + C detector. It consists of a thin (0.020" NE 102) plastic scintillator optically coupled to an ultraviolet transmitting Lucite Cerenkov radiator which in turn is optically coupled to the face of a 7" photomultiplier tube. The pulse height measured from this tube is the integrated light output from the scintillator and the Lucite. This is also analyzed by a 2048 channel pulse height analyzer. The critical parameter for this detector is the ratio of the scintillation to the Cerenkov light, called the S/C ratio, and it has been set from S/C = .2 to S/C = .4 in various flights. (It should be noted that while the S/C ratio has been changed from flight to flight, the element in which the energy of the particle is determined (S_t) has remained unchanged.) The response of this particular detector is dominated above 320 MeV/nucleon by the Cerenkov light which decreases with decreasing energy, whereas below this energy this combination behaves like a pure scintillator.

The final element of the telescope consists of a plastic scintillator called the range detector. This element is used in a "yes-no" manner and provides an energy threshold for particles entering at the top of the telescope of 90 MeV/nucleon for

protons and helium nuclei and 20 MeV for electrons. This divides the particles into two classes -- penetrating, P, and non-penetrating, $\bar{P}$. The telescope as originally designed did not contain either the S_m or P detectors.

The two dimensional response of this instrument, S_t vs S + C, is shown in Figure 2. One can observe from this figure that at energies above 320 MeV/nucleon the simple two dimensional response of the telescope is dominated by the decreasing Cerenkov light output on one axis and the increasing ionization loss on the other. At 320 MeV/nucleon, the Cerenkov threshold, the telescope effectively becomes a double scintillator. The addition of the penetration detector makes it possible to differentiate between high energy helium nuclei and low energy protons and deuterons where their respective response curve cross one another. It also removes electrons < 20 MeV from the minimum ionizing singly charged peak.

The response of this telescope is considered in more detail in Appendix 1 where particular attention is paid to the ways in which the pulse from second scintillator S_m may be used. The principle use of S_m is to provide a consistency check on the ionization loss in S_t. The resultant reduction in background is shown in the appendix along with several sample two dimensional pulse height distributions. Further discussion of the response characteristics of this telescope to various particles will be mentioned as needed.

It should be emphasized that this telescope has sufficient

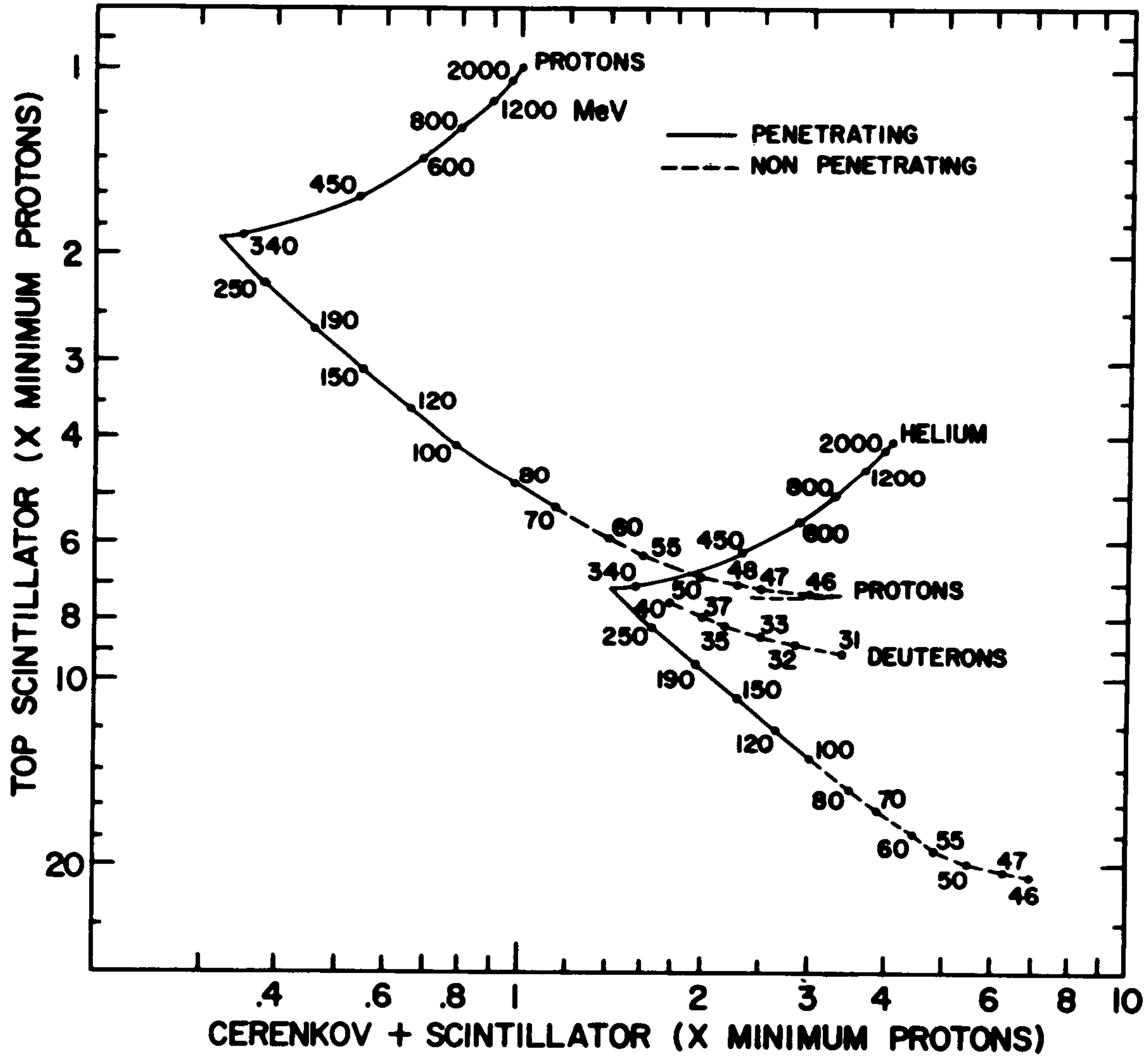
PROTONS
2000
1200 MeV
800
600
450
340
250
190
150
120
100
80
70
60
55
PENETRATING
NON PENETRATING
HELIUM
2000
1200
800
600
450
340
48
47
46
PROTONS
50
40
37
35
33
32
31
DEUTERONS
250
190
150
120
100
80
70
60
55
50
47
46
TOP SCINTILLATOR (X MINIMUM PROTONS)
1
2
3
4
6
8
10
20
CERENKOV + SCINTILLATOR (X MINIMUM PROTONS)
.4
.6
.8
1
2
3
4
6
8
10

Figure 2

collecting area and solid angle (55.4 ster cm^2) and sufficient "resolving power" to observe the time history of spectral changes of protons and helium nuclei with time constants as short as an hour. In the immediate future the telescope can be used to continue observations of the modulation of the cosmic rays both for long term (11 year) and intermediate term (Forbush decrease and diurnal and semi-diurnal variations) effects, to examine the spectral history of high energy solar flare particles, and to look for any as yet unobserved short term effects.

III. DATA ANALYSIS

Many difficulties arise when one attempts to determine the proton and helium differential energy spectra to an accuracy of 5% between 200 MeV/nucleon and 2 BeV/nucleon. First of all extreme care must be taken in the determination of all those quantities which enter into the calculation of a flux, ie. the geometrical factor, the time, the altitude, etc. In addition the energy calibration must be carefully determined and the problem of correcting for statistical fluctuations in energy loss must be solved.

At lower energies, < 200 MeV/nucleon, the accuracy of the proton spectra is completely determined by the correction which must be made for splash and re-entrant (where applicable) albedo and for secondary protons produced both locally and in the overlying atmosphere.

The handling of some of these problems has been considered in a previous work (Ormes, 1965) and here our attention will be directed primarily to the problem of ionization loss fluctuations and their effect on the energy spectrum, the energy calibration and the corrections for albedo and secondary atmospheric protons.

a.) Background

With the latest version of the telescope, two methods are available for determining the corrections for background events lying in regions of particle response on the pulse height distribution. These background events are caused primarily by

nuclear interactions of the cosmic rays with the material in the telescope. As discussed in Appendix 1, discrimination against such interaction events is made by requiring that the two scintillator pulse height measurements be consistent. This provides a method for removing the background according to one of the following criteria:

$$|S_t - S_m| < |S_t + S_m| \, k_1, \; k_1 = 0.3$$

$$|S_t - S_m| < k_2, \; k_2 = 32$$

An alternative method for determining this background (the one used before S_m was introduced) is to extrapolate across regions of particle response from regions of the pulse height distribution which contain only background events. An example of this technique is shown in Figure 3. In this figure a cut through the distribution is taken at S_t = 4x minimum for both P and $\bar{P}$ particles separately. The relativistic helium peak is clearly seen in penetrating particles and is absent in non-penetrating particles. The shape of the background distribution is found to be independent of whether the event was P or $\bar{P}$.

The background as determined by using selection criteria on the S_t and S_m pulses and by the extrapolation method give background corrections consistent to within 10%. This makes the final errors due to background effects of the order of 1% at all energies.

b.) Statistical Fluctuations

The method by which we take account of Landau fluctuations in energy loss is one suggested by the work of Jenkins (1966) on

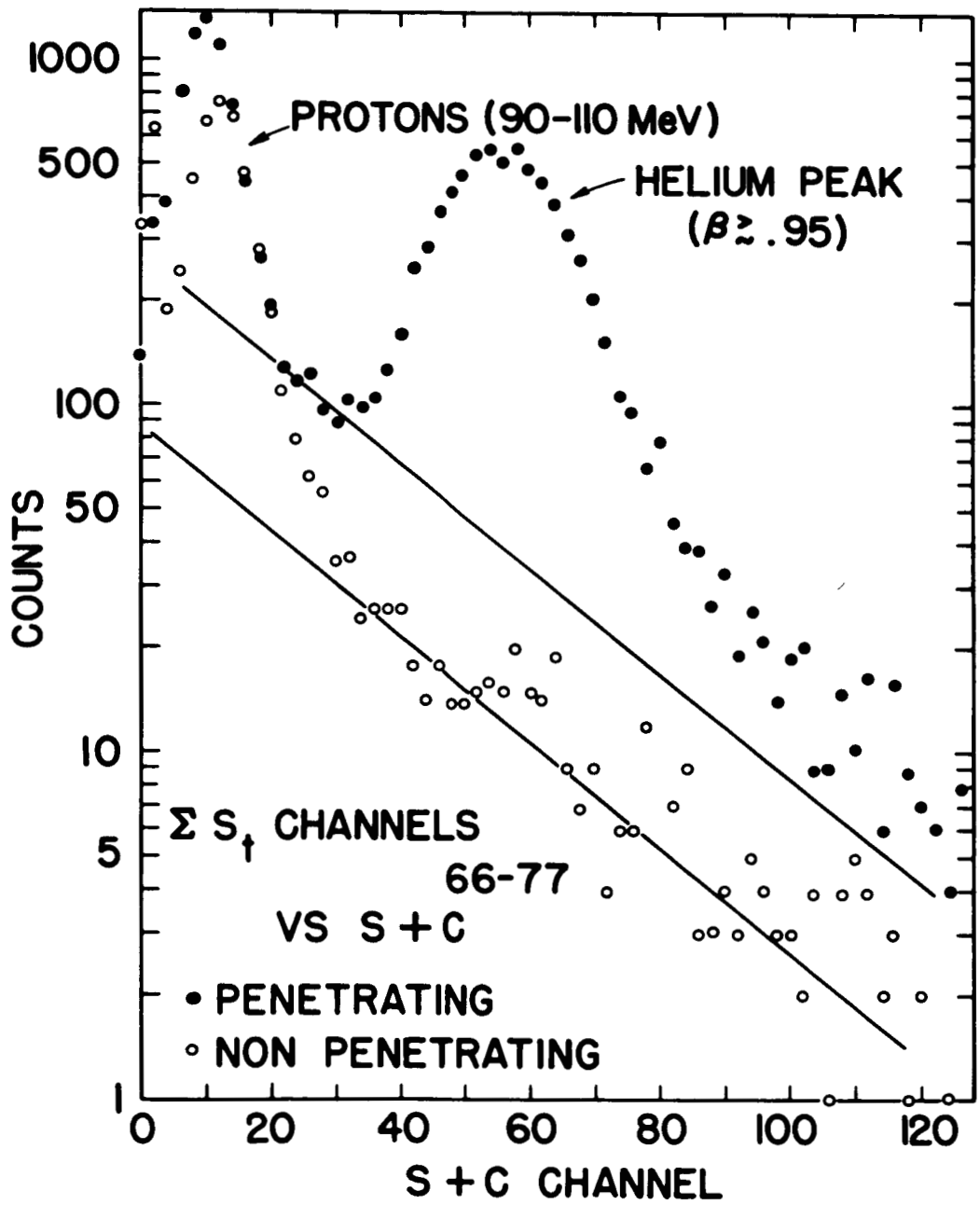
1000
500
100
50
10
5
1
COUNTS
PROTONS (90-110 MeV)
HELIUM PEAK
(β ≳ .95)
Σ S_t CHANNELS
66-77
VS S + C
• PENETRATING
○ NON PENETRATING
0
20
40
60
80
100
120
S + C CHANNEL

Figure 3

cosmic ray spectra and of Subrahmanyan and Ammiraju (1964) on gamma ray spectra.

The problem is to determine the shape of the response function of the telescope to particles of all energies. By far the most important contribution to this response and hence to the final resolution of the detector (as measured by the full width at half maximum - FWHM), are the so called Landau fluctuations (1944).

These statistical fluctuations have been considered in more detail and for a larger range of energies by Symon (1948), hence we will adopt the name Symon statistics for these fluctuations. They represent statistical fluctuations in the energy loss of incident particles traversing thin slabs of matter and are related to the probability of the incident particle producing one or more high energy knock-on electrons. (A thin slab is defined by Symon as one in which a particle loses less than 10% of its total energy.) In the limit of thick crystals the statistical distributions of energy losses becomes Gaussian in shape and is centered at the <u>average</u> ionization loss

$$E_{ave} = \int_0^T \frac{dE}{dt}\, dt \qquad (1)$$

(T is the thickness of the crystal and t is distance measured in gm/cm^2) where dE/dt is the familar Bethe-Block formula

$$\frac{dE}{dt} = -\frac{AZ^2}{\beta^2}\left[\ln \frac{2(m_e c^2)^2 \beta^4}{(1-\beta^2)^2 I^2(z)} - 2\beta^2 - \delta\right] \qquad (2)$$

Here $A = 2\frac{z}{a} N_o\, r_e^2 m_e c^2$, and I(z), the average ionization potential, depend upon the charge z and the mass a of the target material.

($A = 0.0833$ MeV·gm^{-1}cm^2 and $I(z) = 62.6$ eV for NE 102 scintillator.) β is the familar velocity in units of the velocity of light. δ represents a correction for the density effect as evaluated by Sternheimer (1956).

For the whole of the energy range under consideration the telescope contains "thin" elements in which the measured quantity is the most probable energy loss, E_p. In the limit of perfect detector resolution (no fluctuations except Symon statistics) the maximum in the distribution of measured energy losses, E_p, is given by Symon (1948) and Sternheimer (1953) as follows:

$$E_p = \frac{ATZ^2}{\beta^2}\left[\ln\frac{ATZ^2}{\beta^2} + \ln\frac{2m_e c^2\beta^2}{I^2(z)(1-\beta^2)} - \beta^2 + j(\beta,Z) - \delta\right] \quad (3)$$

For any actual detector the peak in the measured energy loss distribution will lie between the values given by formulas (1) and (3). The poorer the resolution of the detector itself the closer the most probable response will approach E_{ave}. (This makes the energy calibration of a detector dependent upon its resolution, a point to which more attention will be directed below.) At minimum ionization (3 BeV/nucleon) E_{ave} and E_p differ by 15% for a 1 gm/cm^2 thick detector and so this effect cannot be ignored. At low energies E_p approaches E_{ave} independent of resolution.

However, we need to know more than the location of the peak in the distribution as a function of energy. The shape of the response distribution of the detector for all particle energies must also be known so that the fraction of counts at any one energy which, due to statistical fluctuations, appear as counts

at some other energy can be determined.

These response distributions may be found using convolution techniques. Let R(E,x) be the composite response distribution of the telescope taking into account both Symon statistics and instrumental effects. E is the particle's energy as it enters the detectors and x is the pulse height measured. This is composed of S(E,x) which is the energy loss distribution function determined by Symon (1948) and of $G_\gamma(x)$ which represents the intrinsic detector response for resolution γ (FWHM). The composite response distributions are then obtained using the convolution integral:

$$R(E,x) = \int_0^\infty S(E,y)\ G_\gamma(x-y)dy \qquad (4)$$

Since the Symon fluctuations of particle energy loss are presumably known (a point to which more attention is directed in the appendix) it remains to determine the intrinsic telescope response function G_γ. It is known from independent studies that fluctuations in the phototube outputs related to photoelectron statistics form an important contribution to the intrinsic response and so one assumes that Gaussian distributions may be used to represent the detector fluctuations (see Mead and Martin, 1965).

It might appear that in making this assumption, effects such as nonuniformity of light collection and path length variations for different particle trajectories are not being considered but this is not the case. The shapes of the pulse height distributions related to these two effects are sufficiently symmetric and well behaved so that when convoluted with typical photoelectron distributions they give slightly broader distributions which are still

essentially Gaussian in shape. Thus the intrinsic detector resolution can be completely represented by a single simple function G_γ.

An example of the convolution in equation (4) is shown in Figure 4. The energy loss distribution S(3.0 BeV,x) is the narrower curve. This is convoluted with a Gaussian of FWHM = 20% ($G_{20\%}$) to give the broader response function. Note particularly that the half-widths of G and S do <u>not</u> add exactly as the square root of the sum of the squares, and that the peak of the convoluted distribution lies between the pulse heights which correspond to the most probable and average light outputs which are at 1.0 and 1.12 x minimum respectively.

The composite response functions can be compared with pulse height distributions measured at sea level where mostly minimum ionizing particles are present. In this way the parameters appropriate to the intrinsic (Gaussian) distribution for a particular detector configuration may be obtained. As can be seen from the example in Figure 5, the composite or convoluted response distribution found in this manner can be fit quite well to the sea level distributions except at large energy losses. A small flux of low energy protons present at sea level is believed to be responsible for the observed deviations.

The composite distributions R(E,x) are then utilized in the following way. A differential number distribution of pulse heights, call it $\frac{dM(x)}{dx}$, is actually measured in a single detector. However, we wish to obtain the differential energy spectrum of the particles

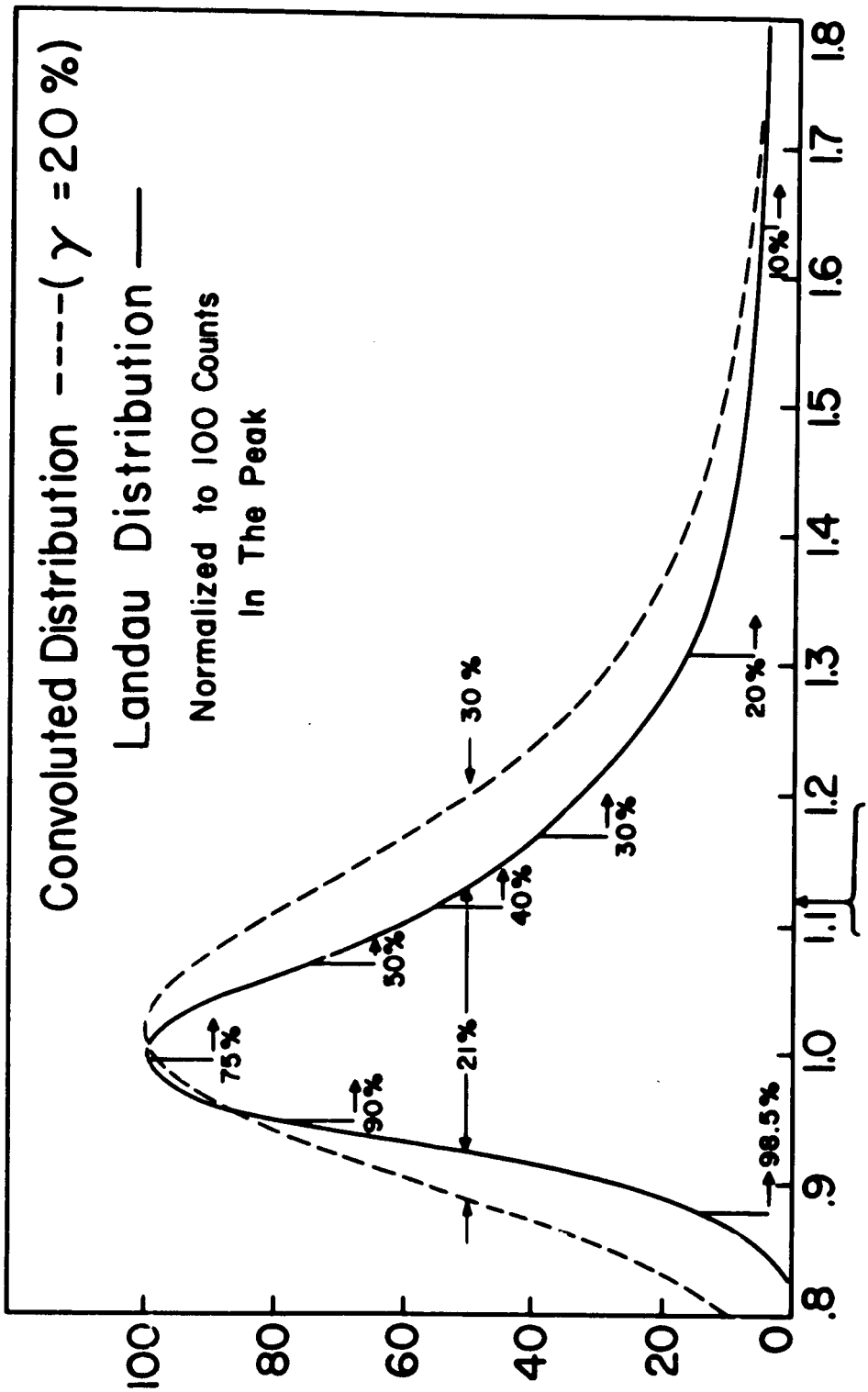
Convoluted Distribution ----(γ =20 %)
Landau Distribution ——
Normalized to 100 Counts
In The Peak
100
80
60
40
20
0
.8
.9
1.0
1.1
1.2
1.3
1.4
1.5
1.6
1.7
1.8
E ave Energy Loss (Ep)
(x minimum)
75%
90%
50%
21%
40%
30%
30 %
20%
10%
98.5%

Figure 4

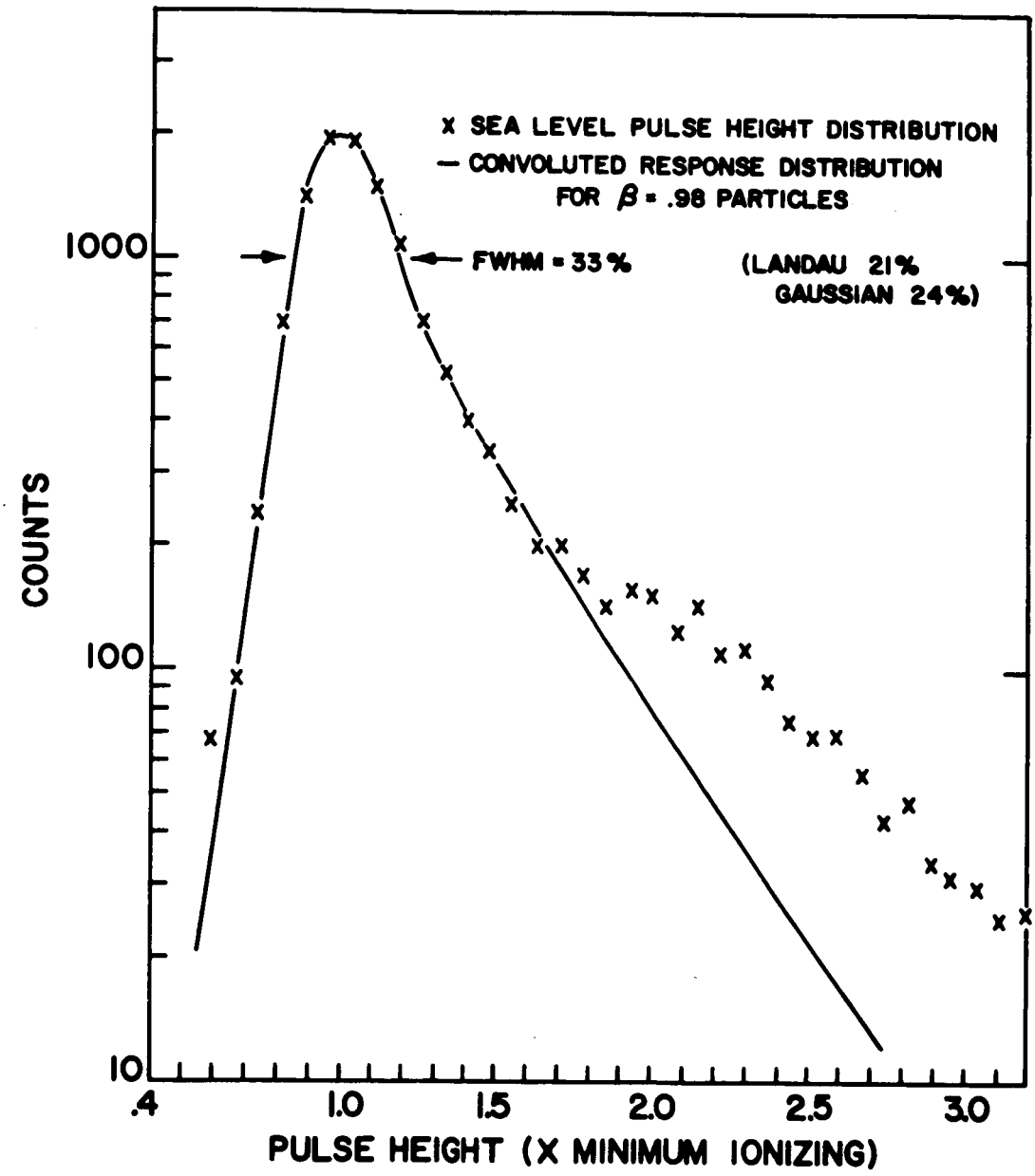
X SEA LEVEL PULSE HEIGHT DISTRIBUTION
— CONVOLUTED RESPONSE DISTRIBUTION FOR β = .98 PARTICLES
FWHM = 33%
(LANDAU 21% GAUSSIAN 24%)
COUNTS
1000
100
10
.4
1.0
1.5
2.0
2.5
3.0
PULSE HEIGHT (X MINIMUM IONIZING)

Figure 5

entering the detector, $\frac{dj}{dE}(E)$. These two are not simply related, and the problem becomes one of solving the integral equation

$$\frac{dM(x)}{dx} = \int_0^\infty \frac{dj(E)}{dE} \int_0^\infty S(E,y)\, G(x-y)\, dy\, dE$$

$$= \int_0^\infty R(E,x)\, \frac{dj(E)}{dE}\, dE \qquad (5)$$

The description of the methods by which the two dimensional pulse height distributions yield an energy spectrum dj(E)/dE, ie. the solution of equation (5), is considered in detail in Appendix 2. Suffice to say here that the integral equation is replaced by a finite sum, with each of the ten pulse height intervals into which this scale is divided corresponding to an energy interval. The resultant system of ten coupled equations has the measured differential pulse height spectrum as the known quantity and the desired differential energy spectrum as the unknown. This system is solved by the iterative procedure described in the appendix.

In Figure 6 an energy spectrum obtained directly from a pulse height spectrum is compared to an energy spectrum obtained after considering the response functions and solving equation(5). The differences between these two spectra become important above about 200 MeV/nucleon.

c.) Energy Calibration

Let us direct our attention now to the energy calibration of the detector. As mentioned in the above discussion the most probable light output of a detector for particles of a given energy depends upon resolution of the detector and lies between E_p and E_{ave}.

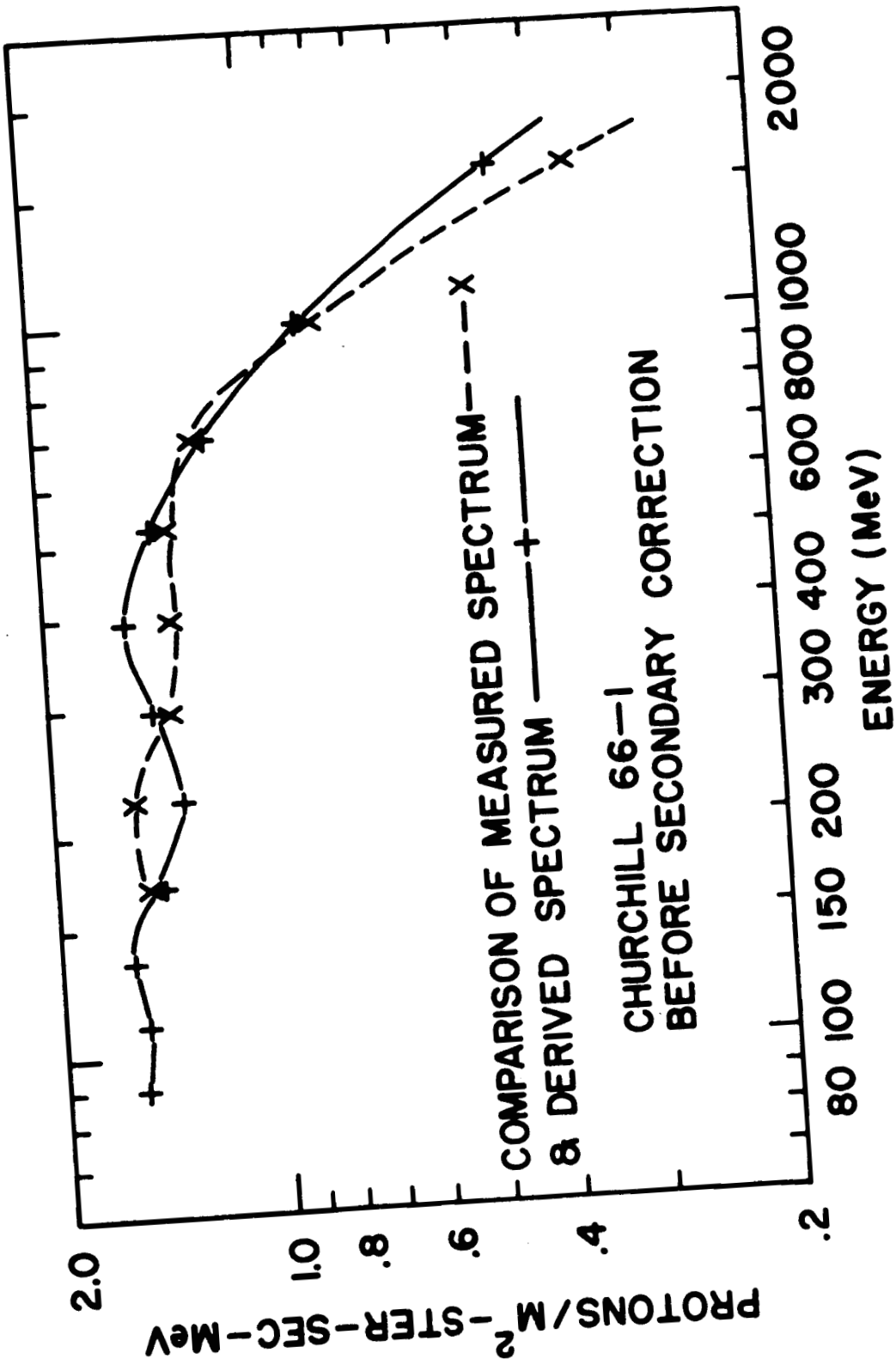
PROTONS/M²-STER-SEC-MeV
2.0
1.0
.8
.6
.4
.2
80 100 150 200 300 400 600 800 1000 2000
ENERGY (MeV)
COMPARISON OF MEASURED SPECTRUM---X
& DERIVED SPECTRUM ——+——
CHURCHILL 66-1
BEFORE SECONDARY CORRECTION

Figure 6

In view of this and because of the non-linear relationship of energy loss to light output for plastic scintillators it is extremely valuable to have the energy scale internally calibrated. In this telescope we have three energy calibration points for protons and helium nuclei: (1) the minimum ionizing peak, (2) the Cerenkov threshold of 320 MeV/nucleon and (3) the 91 MeV/nucleon point defined by the range detector. These energies and the relativistic peaks for charges through Z = 10 enable us to determine the non-linearities present in the plastic scintillator as a function of both particle velocity and charge.

Expressing the non-linearity in a form that follows the work of Birks (1951) the most probable light output is written as $L_p = \frac{(1 + k_1)\ E_p}{1 + k_1\ E_p}$ where the constant k_1 depends upon particle charge. Values of $k_1 = 0.019 \pm 0.002$ MeV^{-1} for protons and $k_1 = 0.013 \pm 0.002$ MeV^{-1} for helium nuclei have been derived from the data. As a result of the charge dependence of the constant k_1, a proton will give slightly less light output than will a helium nucleus at the same value of energy loss, ie. when $\beta_p = 1/2\ \beta_{He}$. Previous work using the relativistic higher Z charge peaks to determine the non-linearity (Ormes, 1965, and Webber and Ormes, 1967 b) yielded a first order non-linearity coefficient of $k_1 = 0.010 \pm 0.001$ gm cm^{-2}/MeV.

A similar charge dependence of the non-linearity coefficients in NE 102 plastic scintillator has been examined in detail by Badhwar et al., (1967 a). Their energy range (40 to 200 MeV/nucleon) is different from ours and they use the differential relationship

$$\frac{dL}{dx} = \frac{S(dE/dx)}{1+kB(dE/dx)}$$

and obtain values of kB = 0.0126 $\pm$ 0.002 gm/(cm^{2}MeV) for protons and 0.0072 $\pm$ 0.001 gm/(cm^{2}MeV) for helium. The value of kB in their differential expression is directly comparable to k_1 in our integral expression because our detector is 1 gm/cm^2 thick. They explain the charge dependence by saying that for helium nuclei a larger fraction of the deposited energy is carried away from the dense ionization column (saturation region) by high energy knock-on electrons (delta rays).

The requirement that the spectra derived separately from S_t and S_m be identical assures that the non-linearities have been properly accounted for and that no systematic distortions remain in the energy calibration.

d.) Atmospheric Corrections

Because of the large number of flights made at various latitudes, altitudes and levels of solar modulation, considerable information is available on the atmospheric secondary and re-entrant albedo proton fluxes.

In Figure 7 we present the re-entrant albedo spectrum deduced from the flights made at Fayetteville and Ely. Since these flights were at nearly the same depth (6.6 and 6.0 gm/cm^2) the two spectra can be directly compared. Note the effect of the geomagnetic cut-off at Ely. Above the cut-off energy of 340 MeV little splash albedo originating in the southern hemisphere is trapped, hence there is no re-entrant albedo above

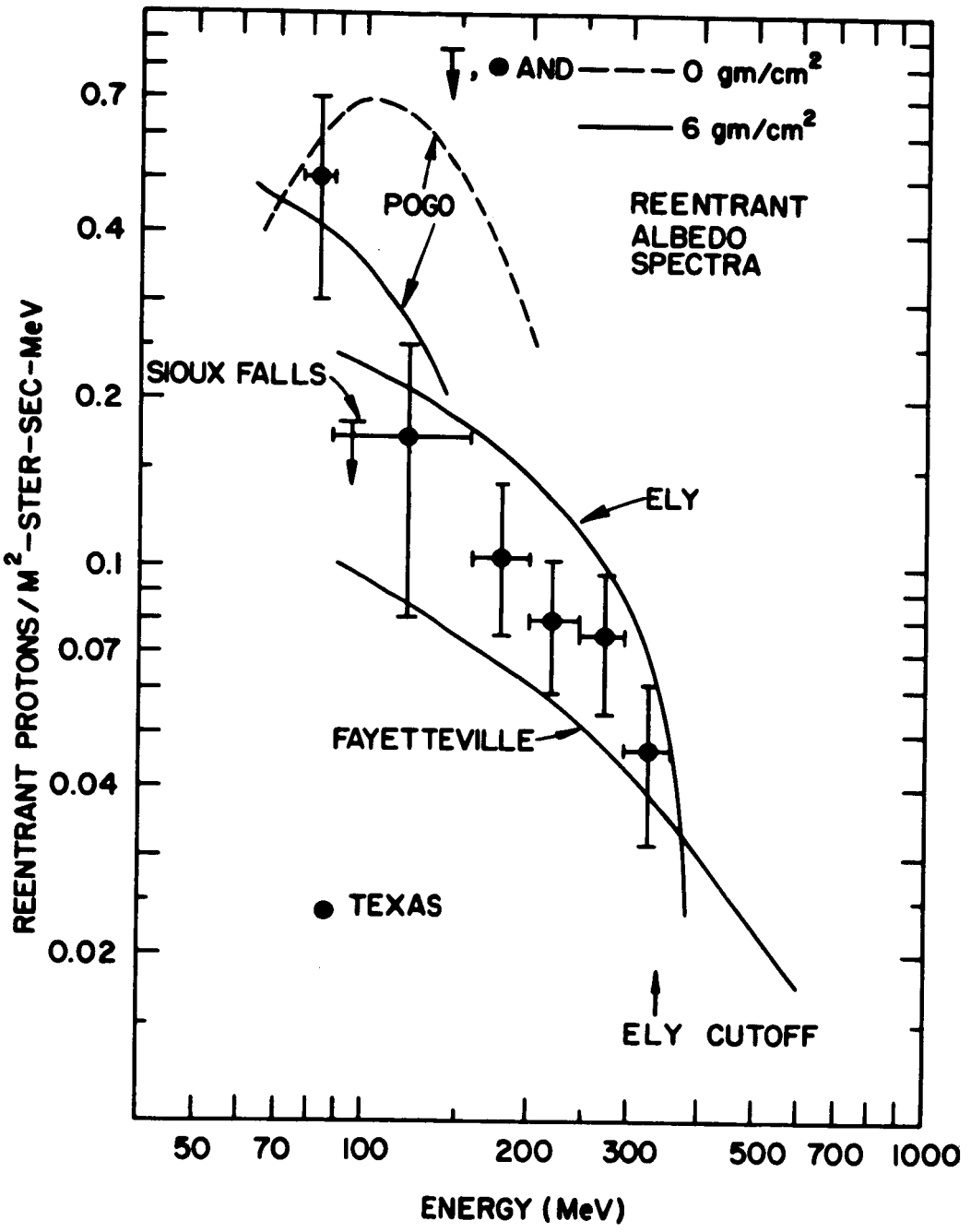
, ● AND
0 gm/cm²
6 gm/cm²
REENTRANT ALBEDO SPECTRA
POGO
SIOUX FALLS
ELY
FAYETTEVILLE
● TEXAS
ELY CUTOFF
REENTRANT PROTONS/M²-STER-SEC-MeV
0.7
0.4
0.2
0.1
0.07
0.04
0.02
50
70
100
200
300
500
700
1000
ENERGY (MeV)

Figure 7

this energy. On the other hand at Fayetteville, where the cut-off is 2200 MeV, the albedo spectrum is roughly proportional to $1/E^{1.5}$. Above 600 MeV it becomes a negligible correction.

Comparing the relative intensities of re-entrant albedo below 250 MeV at Ely and Fayetteville, we find that the re-entrant albedo intensity is roughly proportional to the total integral intensity of primary protons above 200 MeV at each location. This primary proton intensity at Fayetteville is 1130 particles/m^2-ster-sec and at Ely is 2710 particles/m^2-ster-sec. The re-entrant intensities at Ely are also a factor of 2.4 larger than at Fayetteville.

With this prescription in mind for the correction to other latitudes and levels of modulation, this data can be compared with that of other workers. First of all, there is the upper limit at 0 gm/cm^2 given by Teegarden (1967) at Sioux Falls. When this measurement is adjusted for the difference in intensity between 1961, when his flight was made, and our intensities, this upper limit is consistent with our measurements. The data of Verma, also appropriate to 0 gm/cm^2, at Palestine, Texas (1966) agrees quite well with the Fayetteville data when the latter is extrapolated to 0 gm/cm^2. In this case the difference in latitude of the two measurements is compensated by the difference in level of solar modulation, the flights of Verma being made in 1965 at a time near the maximum in cosmic ray intensity.

Also shown is a measurement by Sawyer et al., (1967) obtained with an instrument quite similar to ours which has been on board

a POGO satellite. Their albedo spectrum outside of the atmosphere at an L value ≃ 4 (dashed curve Figure 7) may be compared to our measurement at Ely by passing the POGO spectrum through 6 gm/cm^2 of atmosphere (solid curve marked POGO). Intensities of these two spectra agree reasonably well.

Now let us turn our attention to the secondary protons. In Figure 8, the secondary proton spectrum (includes deuterons and tritons as well) deduced at an atmospheric depth, of 3 gm/cm^2, (flight Churchill 65-2) is shown. This flight was made when the Mt. Washington neutron monitor was within 2% of its sunspot minimum value and the integral flux of primary protons above 200 MeV was 2850 particles/m^2-ster-sec. At the latitude of Churchill the cut-off is less than 20 MeV so that we can ignore re-entrant albedo protons.

The secondary proton correction that has been applied at other latitudes and levels of solar modulation is obtained as follows: We assume the secondary protons are due to interactions of cosmic rays in the overlying atmosphere, and at depths $\leq$ 6 gm/cm^2 and above 100 MeV, the intensity of secondaries will be directly proportional to the amount of overlying atmosphere, (see Hofmann and Winckler, 1967). The work of Webber and Ormes (1967 a) suggests that the efficiency of primary cosmic rays for producing low energy secondary protons is nearly independent of the energy of the primary above ≃ 200 MeV/nucleon. We therefore assume that the intensity of secondary protons is proportional to the total primary intensity above 200 MeV/nucleon.

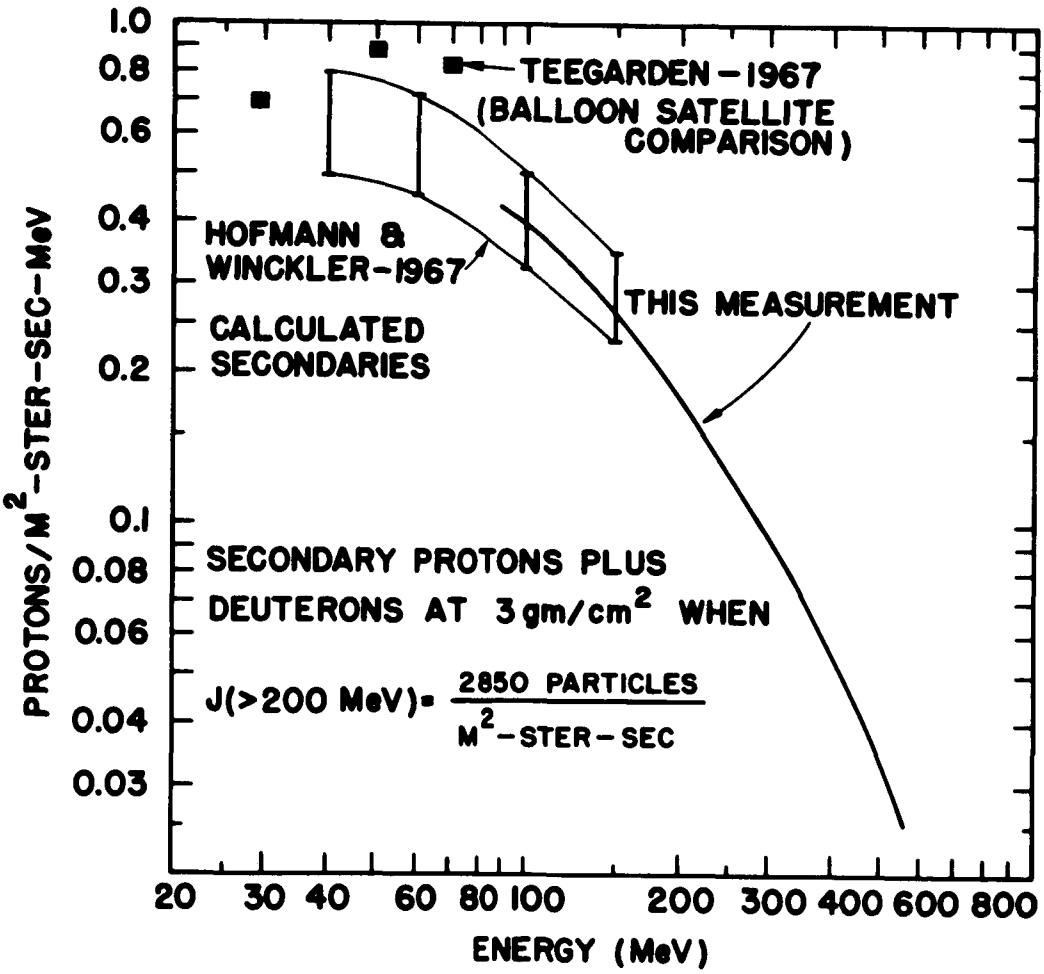
1.0
0.8
0.6
0.4
0.3
0.2
0.1
0.08
0.06
0.04
0.03
PROTONS/M²-STER-SEC-MeV
TEEGARDEN – 1967
(BALLOON SATELLITE
COMPARISON)
HOFMANN &
WINCKLER-1967
CALCULATED
SECONDARIES
THIS MEASUREMENT
SECONDARY PROTONS PLUS
DEUTERONS AT 3 gm/cm² WHEN
J(>200 MeV) = 2850 PARTICLES / M²-STER-SEC
20 30 40 60 80 100 200 300 400 600 800
ENERGY (MeV)

Figure 8

The secondary proton spectrum we obtain agrees quite well with the calculations of Hofmann and Winckler (1967) when their calculated spectrum at 5 gm/cm^2 is adjusted to 3 gm/cm^2 depth. Teegarden (1967) has obtained results at a slightly lower energy by making a direct comparison of simultaneous measurements of the proton spectrum on the IMP satellite and at Churchill using balloons.

Teegarden reports that he is unable to detect any variations of the intensity of atmospheric secondaries with solar cycle from 1961 to 1964 at Sioux Falls. We do observe a slight decrease (10%) in the secondary proton intensity between 1965 and 1966 corresponding to a 3% decrease in neutron monitor intensity. The ability to detect a change of this magnitude serves to emphasize the importance of the large geometrical factor used in this experiment.

e.) Accuracy of the Results

Before discussing the spectra of primary protons and helium nuclei it is worthwhile to say something about the accuracy of the results from this experiment.

It should be emphasized that, because the high counting rates, statistics are a negligible source of error, for helium nuclei as well as for protons. This means that systematic errors, which are more difficult to evaluate, are the dominant source of uncertainty. The following estimates of these errors are believed to be conservative.

At low energies (100-400 MeV/nucleon) the accuracy is limited

by uncertainties in the knowledge of the correction for atmospheric secondaries (and albedo at lower latitudes). The secondary correction is typically 50% of the total proton intensity at 100 MeV and decreases to about 20% at 200 MeV. If this correction is known to $\pm$ 10% then the absolute error in this range may be as large as $\pm$ 5%. Because the corrections are made consistently from one flight to the next, the relative error between flights is much less however, perhaps $\pm$ 2-3%.

At higher energies ($\geq$ 400 MeV/nucleon) the uncertainties in both the proton and helium spectra are determined by the accuracy of the correction for fluctuations of particles from one energy interval to the next. Since this correction to the differential intervals is of order of $\pm$ 20% or less (see Figure 6), the relative intensities deduced for adjacent differential energy intervals are estimated to be accurate to within $\pm$ 5%. The integral accuracy of the various spectra relative to one another is limited by a knowledge of the geometrical factor of the telescope and is about $\pm$ 2%.

IV. SPECTRA OF PRIMARY PROTONS AND HELIUM NUCLEI

Many of the results obtained on this series of flights have been previously reported in preliminary form (see references to Ormes and to Webber), but in this work some minor adjustments and corrections have been made to the data. Because of this, and for the sake of completeness, all of the data collected on protons and helium nuclei will be presented here.

Figure 9 shows a regression plot of the integral intensity of protons above 450 MeV and the Mt. Washington neutron monitor daily average. The good tracking between these two types of instruments confirms that the integral accuracy of the instrument is as advertised ($\pm$ 2%). During this series of measurements the proton intensity above 450 MeV changed by 16.1 $\pm$ 0.9%, while the corresponding change in neutron monitor rate was 5.9 $\pm$ 0.3%. The ratio of changes is thus 2.7 $\pm$ 0.2 for particles of mean energies $\simeq$ 2 BeV and 15 BeV respectively. The two flights made in 1966 after cosmic ray maximum allow us to examine the relative changes during periods of increasing and decreasing solar modulation. There is no evidence to within 2% for any different behavior of the modulation before and after sunspot minimum.

Figure 10 shows a regression plot of the intensity of > 2.0 BeV protons against the neutron monitor rate. The ratio of modulation of these protons of mean energy about 3 BeV to the neutron monitor is 2.35 $\pm$ 0.2. The flight at Fayetteville can be used to check the integral intensities > 2 BeV deduced from the high

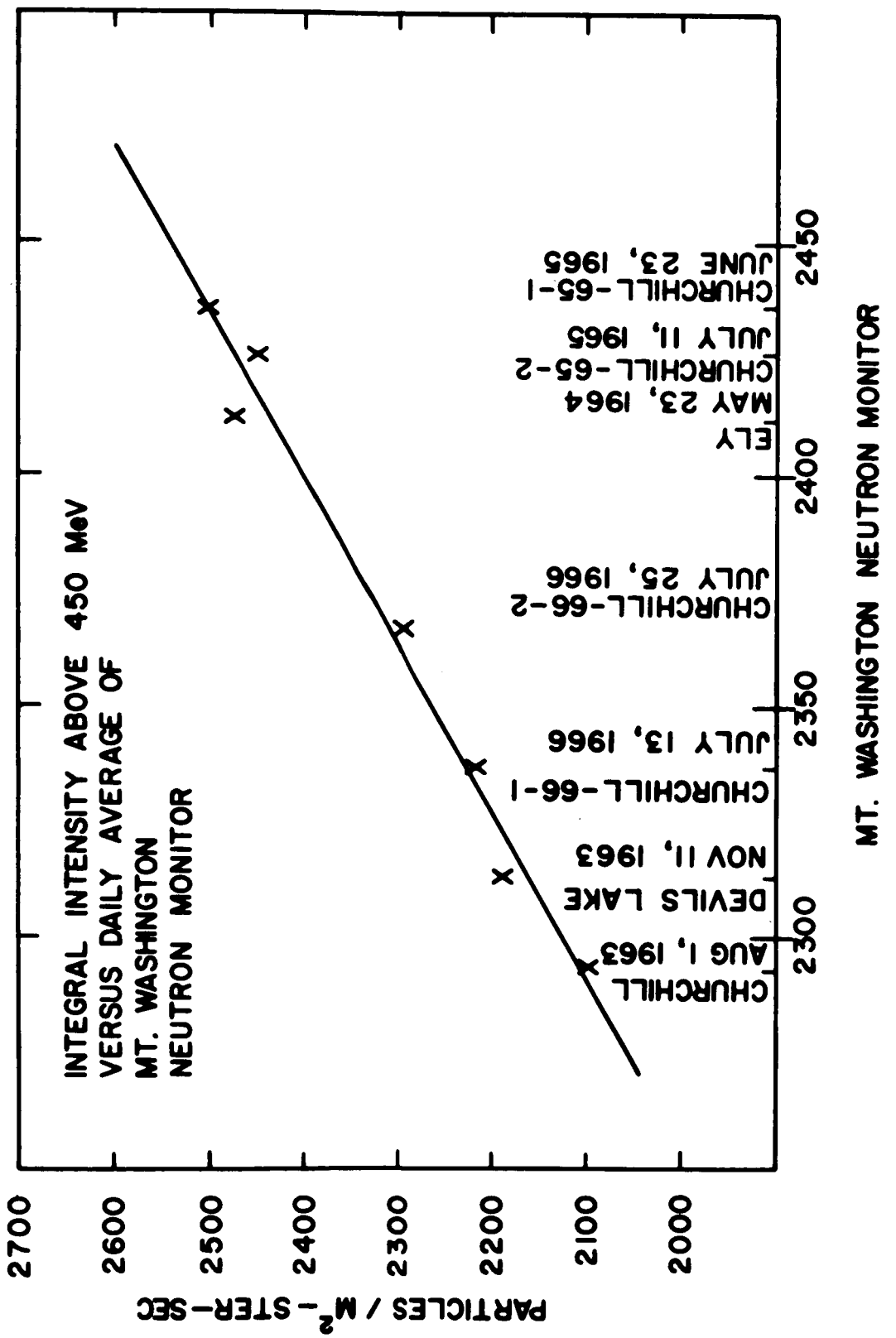
INTEGRAL INTENSITY ABOVE 450 MeV
VERSUS DAILY AVERAGE OF
MT. WASHINGTON
NEUTRON MONITOR
PARTICLES / M²-STER-SEC
2700
2600
2500
2400
2300
2200
2100
2000
2300
2350
2400
2450
MT. WASHINGTON NEUTRON MONITOR
CHURCHILL
AUG 1, 1963
DEVILS LAKE
NOV 11, 1963
CHURCHILL-66-1
JULY 13, 1966
CHURCHILL-66-2
JULY 25, 1966
ELY
MAY 23, 1964
CHURCHILL-65-2
JULY 11, 1965
CHURCHILL-65-1
JUNE 23, 1965

Figure 9

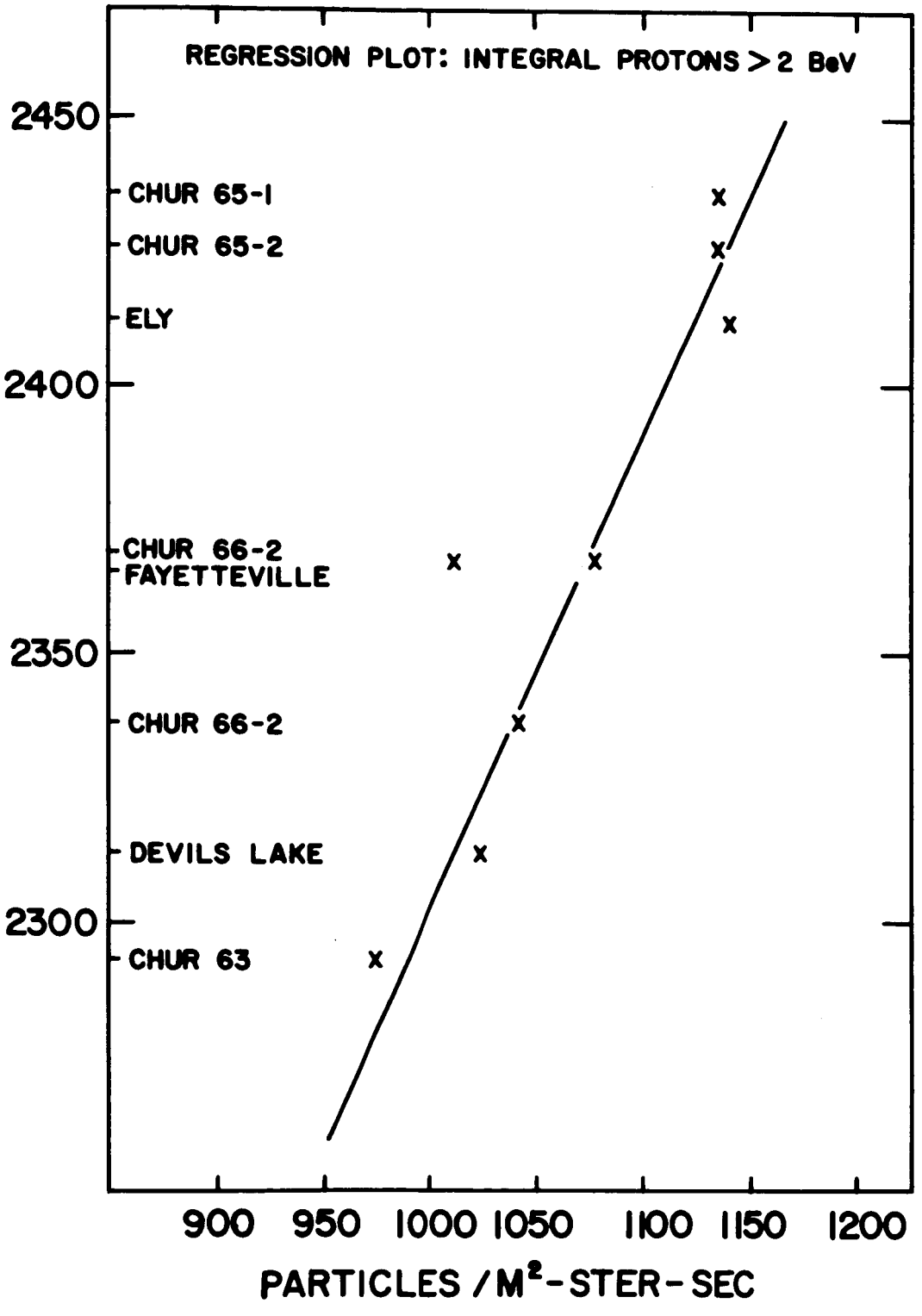
REGRESSION PLOT: INTEGRAL PROTONS > 2 BeV
2450
2400
2350
2300
CHUR 65-1
CHUR 65-2
ELY
CHUR 66-2
FAYETTEVILLE
CHUR 66-2
DEVILS LAKE
CHUR 63
900
950
1000
1050
1100
1150
1200
PARTICLES / M² - STER - SEC

Figure 10

latitude flights. The geomagnetic cut-off at Fayetteville is about 3.0 BV (Shea and Smart, 1967) which is equal to 2150 MeV for protons. We therefore expect that the intensity measured at Fayetteville should lie a few % to the left of the regression line shown. In fact it lies 4% to the left.

The next two figures show the differential proton spectra corrected to the top of the atmosphere. The extrapolation from the balloon depth takes place in two steps. First the intensities are corrected for those protons which have interacted in the telescope (becoming background) or in the air above using an absorption mean free path of 100 gm/cm^2 for air and an interaction mean free path of 75 gm/cm^2 in plastics. Secondly each energy interval is corrected for ionization loss in the matter above the telescope using Sternheimer's (1960) range energy tables for protons in air.

In Figure 11 the spectra for Minneapolis, Devil's Lake and Ely are presented. The effects of the geomagnetic cut-off are clearly visible. A comparison of the measured cut-offs with those to be expected theoretically has been conducted elsewhere (Sawyer et al., 1967). Figure 12 gives the proton spectra for the five flights at Churchill during the 1963-1966 period. Where error bars are shown, they are $\pm$ 5%. It is possible to see a positive correlation of the primary proton intensity with the neutron monitor rate corresponding to changes as small as 1% in the latter. The maximum in the differential spectra can also clearly be seen to be controlled by the degree of solar

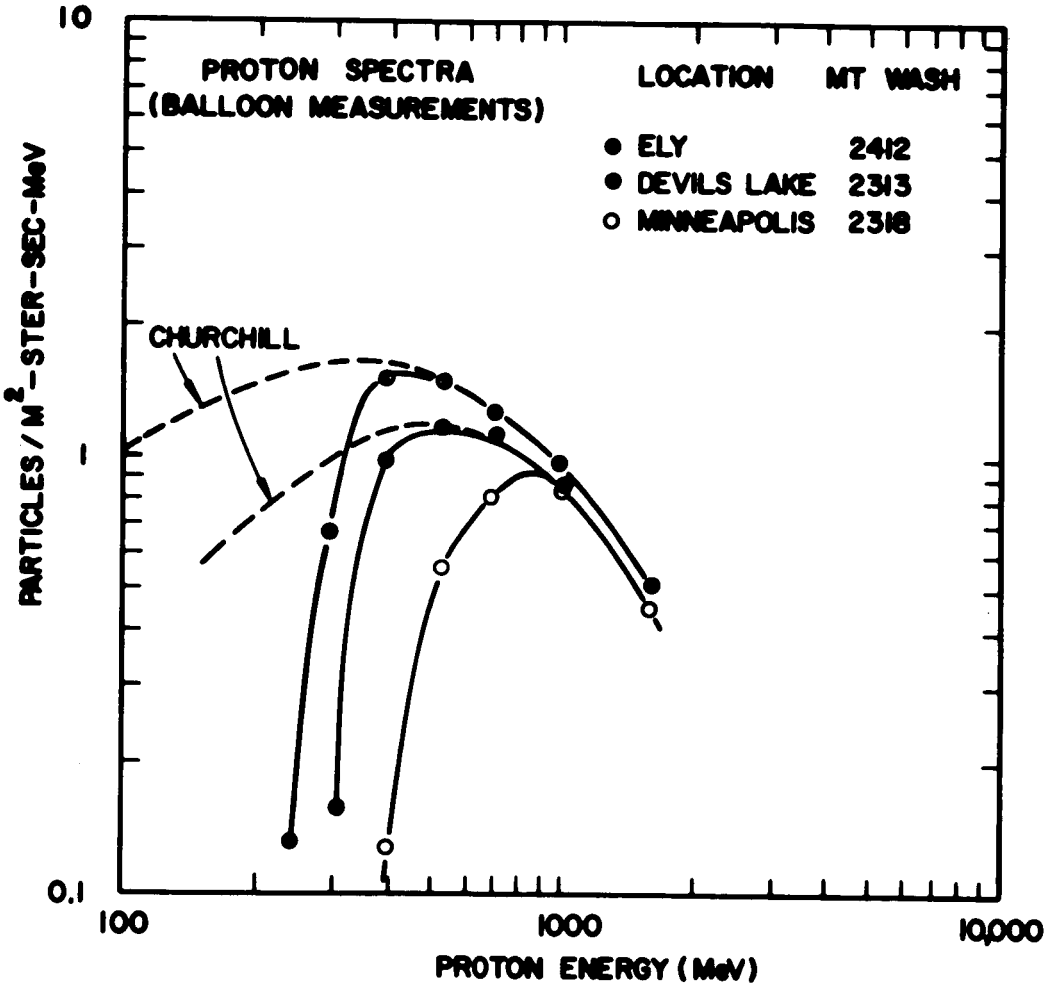
PROTON SPECTRA
(BALLOON MEASUREMENTS)
LOCATION MT WASH
ELY 2412
DEVILS LAKE 2313
MINNEAPOLIS 2318
CHURCHILL
PARTICLES / M²-STER-SEC-MeV
10
1
0.1
100
1000
10,000
PROTON ENERGY (MeV)

Figure 11

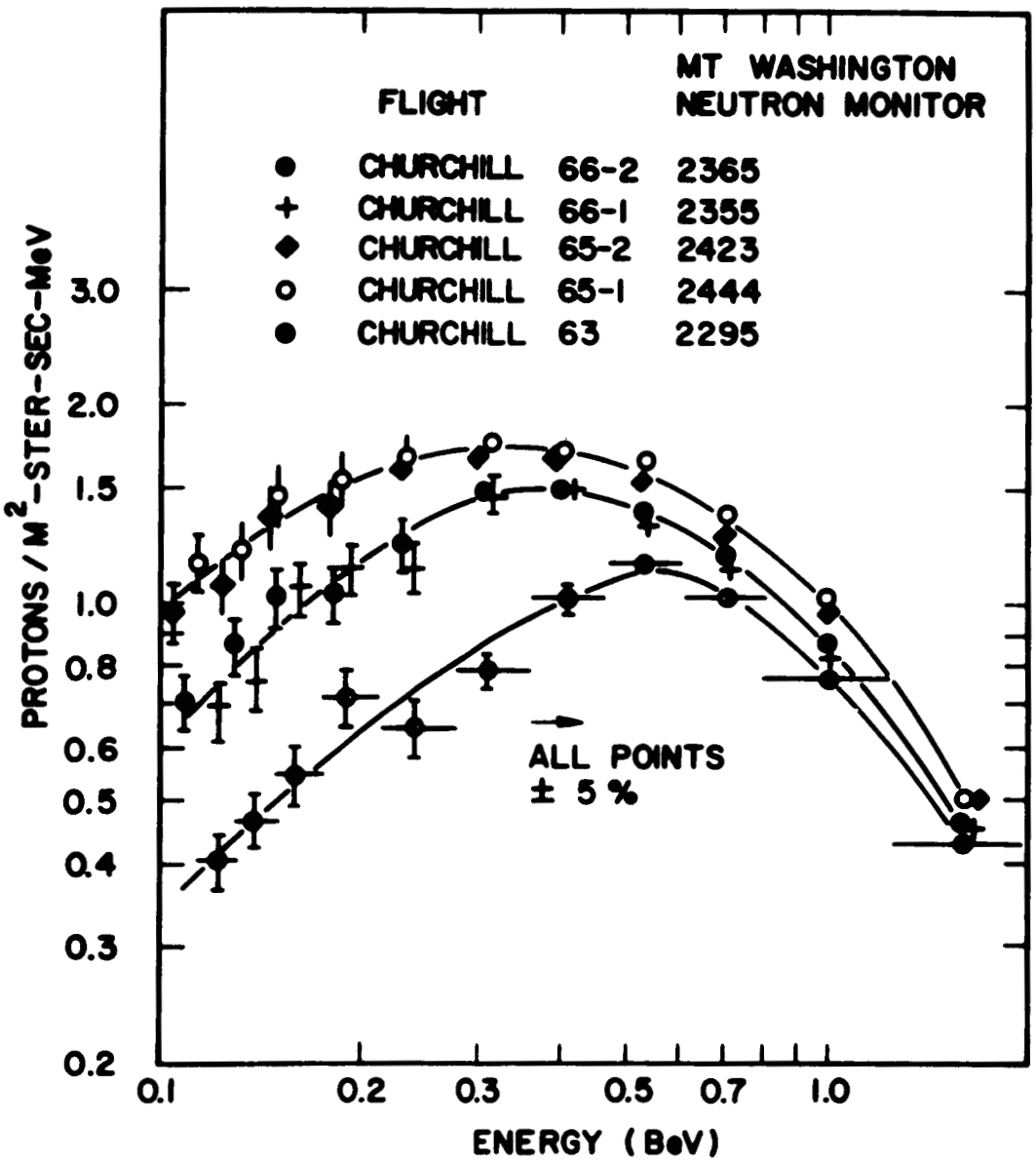
MT WASHINGTON
NEUTRON MONITOR
FLIGHT
CHURCHILL 66-2 2365
CHURCHILL 66-1 2355
CHURCHILL 65-2 2423
CHURCHILL 65-1 2444
CHURCHILL 63 2295
ALL POINTS
± 5 %
PROTONS / M²-STER-SEC-MeV
3.0
2.0
1.5
1.0
0.8
0.6
0.5
0.4
0.3
0.2
0.1
0.2
0.3
0.5
0.7
1.0
ENERGY (BeV)

Figure 12

modulation. It changes from 350 MeV to about 500 MeV during the period of measurement.

The next Figure, 13, shows a regression plot of the intensity of helium nuclei > 450 MeV/nucleon against the neutron monitor rate. Note that the modulation of these particles is definitely less than for protons of a corresponding energy. The change in this integral flux is 1.8 ± 0.2 times the neutron monitor change.

Combining this with the proton data gives a ratio of change of protons to helium nuclei of 1.5 for particles > 450 MeV/nucleon. We will consider the significance of this ratio later after we have developed a theoretical framework within which to discuss the modulation. We can say here that neither of the commonly considered simple functional forms for the modulation, $1/\beta$ (=> $\Delta P/\Delta He$ modulation = 1) and $1/\beta R$ (=> $\Delta P/\Delta He$ modulation = 2), will explain the observed relative modulation of protons and helium nuclei in this energy range.

Next we examine the differential spectra of helium nuclei in the energy range 120 MeV/nucleon to 2 BeV/nucleon corresponding to the proton differential spectra presented above. The helium intensities are corrected to the top of the atmosphere using the attenuation mean free path 53 ± 2 gm/cm^2 as determined directly on the ascent portions of our flights (Ormes and Webber, 1965). The correction for ionization loss is made in the same manner as for protons (assuming all the particles are He^4).

In Figure 14 the helium nuclei spectra obtained at Minneapolis, Devil's Lake and Ely are compared with the spectra from Churchill.

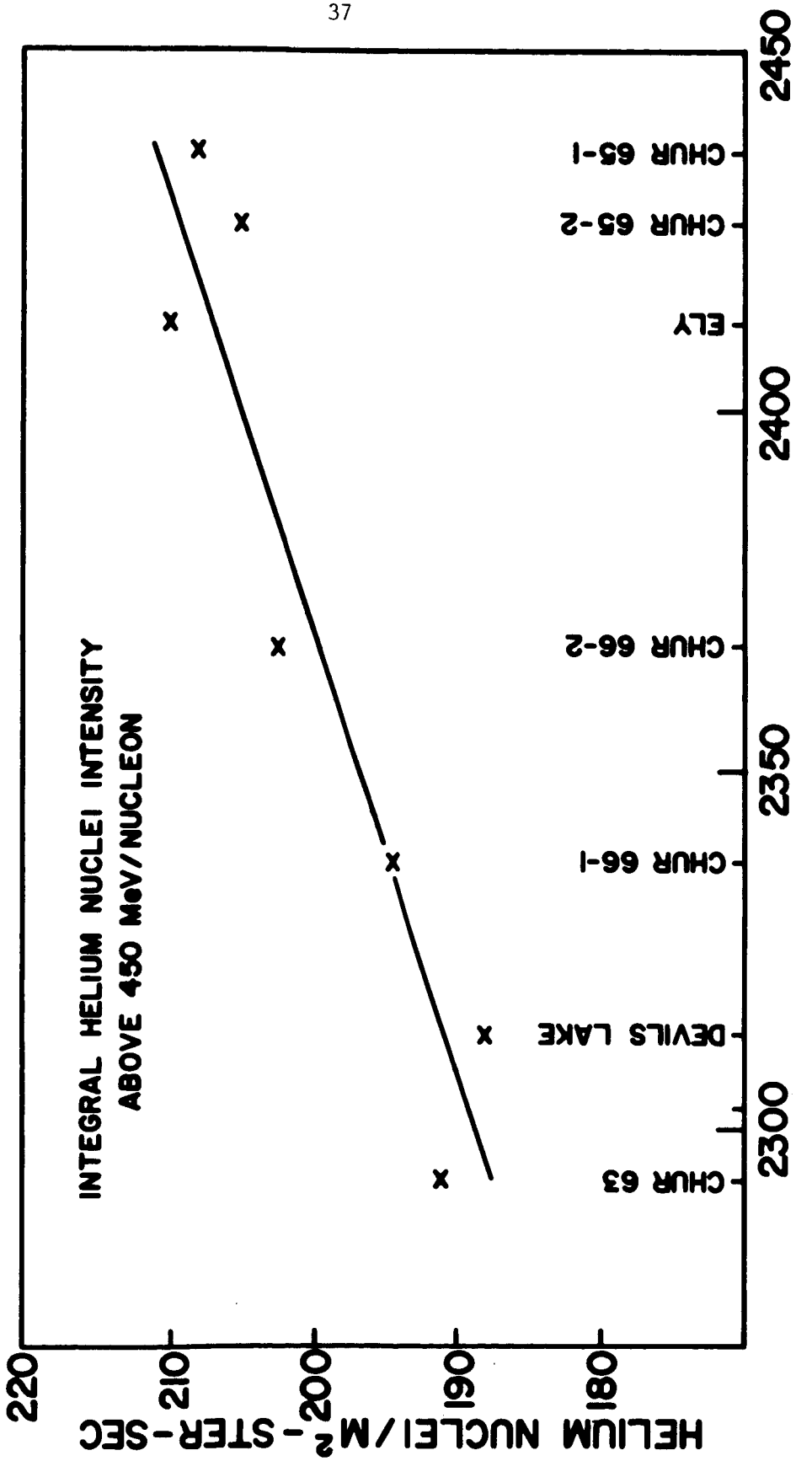
INTEGRAL HELIUM NUCLEI INTENSITY
ABOVE 450 MeV/NUCLEON
HELIUM NUCLEI/M²-STER-SEC
220
210
200
190
180
MT. WASHINGTON NEUTRON MONITOR
2300
2350
2400
2450
CHUR 63
DEVILS LAKE
CHUR 66-1
CHUR 66-2
ELY
CHUR 65-2
CHUR 65-1

Figure 13

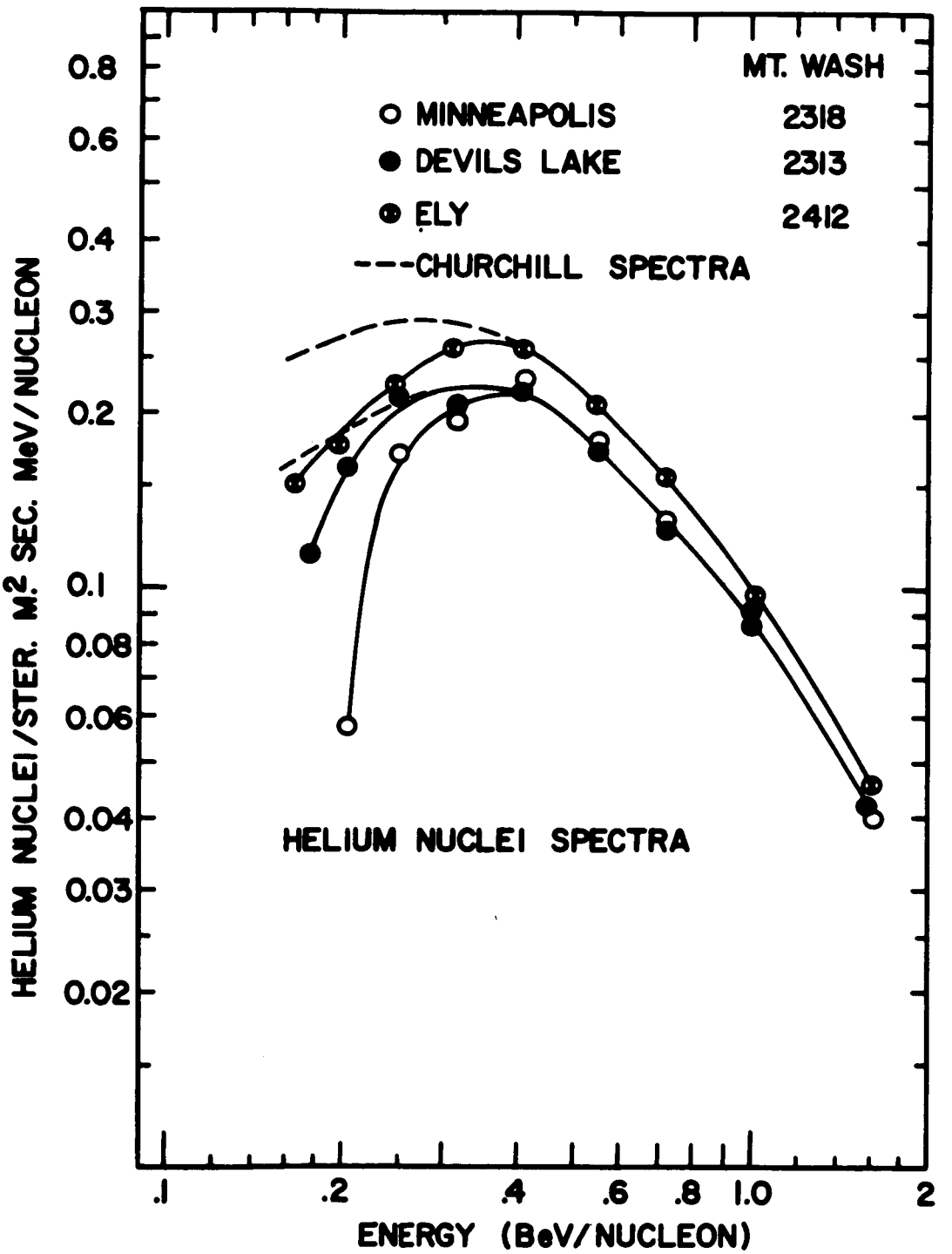
MT. WASH
MINNEAPOLIS 2318
DEVILS LAKE 2313
ELY 2412
---CHURCHILL SPECTRA
HELIUM NUCLEI SPECTRA
HELIUM NUCLEI/STER. M.² SEC. MeV/NUCLEON
0.8
0.6
0.4
0.3
0.2
0.1
0.08
0.06
0.04
0.03
0.02
.1
.2
.4
.6
.8
1.0
2
ENERGY (BeV/NUCLEON)

Figure 14

The effects of the geomagnetic cut-off can again be seen by noticing the break-away from the high latitude spectra.

The five helium nuclei spectra measured at Churchill are presented in Figure 15. It is immediately obvious that these nuclei are undergoing less modulation than protons at the same energy/nucleon, in accordance with our expectations based on the integral measurements just discussed.

Before turning our attention to the details of this solar modulation, we shall compare the spectra just presented with those of other workers. This is done first for protons in Figure 16. The results of Freier and Waddington (1965) which cover an energy range comparable to our own (but are not comparable statistically and therefore are not shown) verify the shape of the spectra presented here quite well. Balasubrahmanyan and McDonald (1964), also obtained some points which are neither as extensive nor as accurate from a balloon flight in 1963. A separate NASA balloon measurement (Teegarden, 1967) at lower energy was made in 1963 at nearly the same neutron monitor level as our flight and fits smoothly on to our low energy data.

No Churchill flights were made in this series during 1964, but the 1966 flights correspond to a neutron monitor rate approximately half-way between 1963 and 1965. This data is comparable to the low energy data of the NASA group, taken on the IMP satellite in early 1964, (Balasubrahmanyan et al., 1967). The spectra join smoothly and quite reasonably together at about 100 MeV. Some balloon measurements by the Rochester group

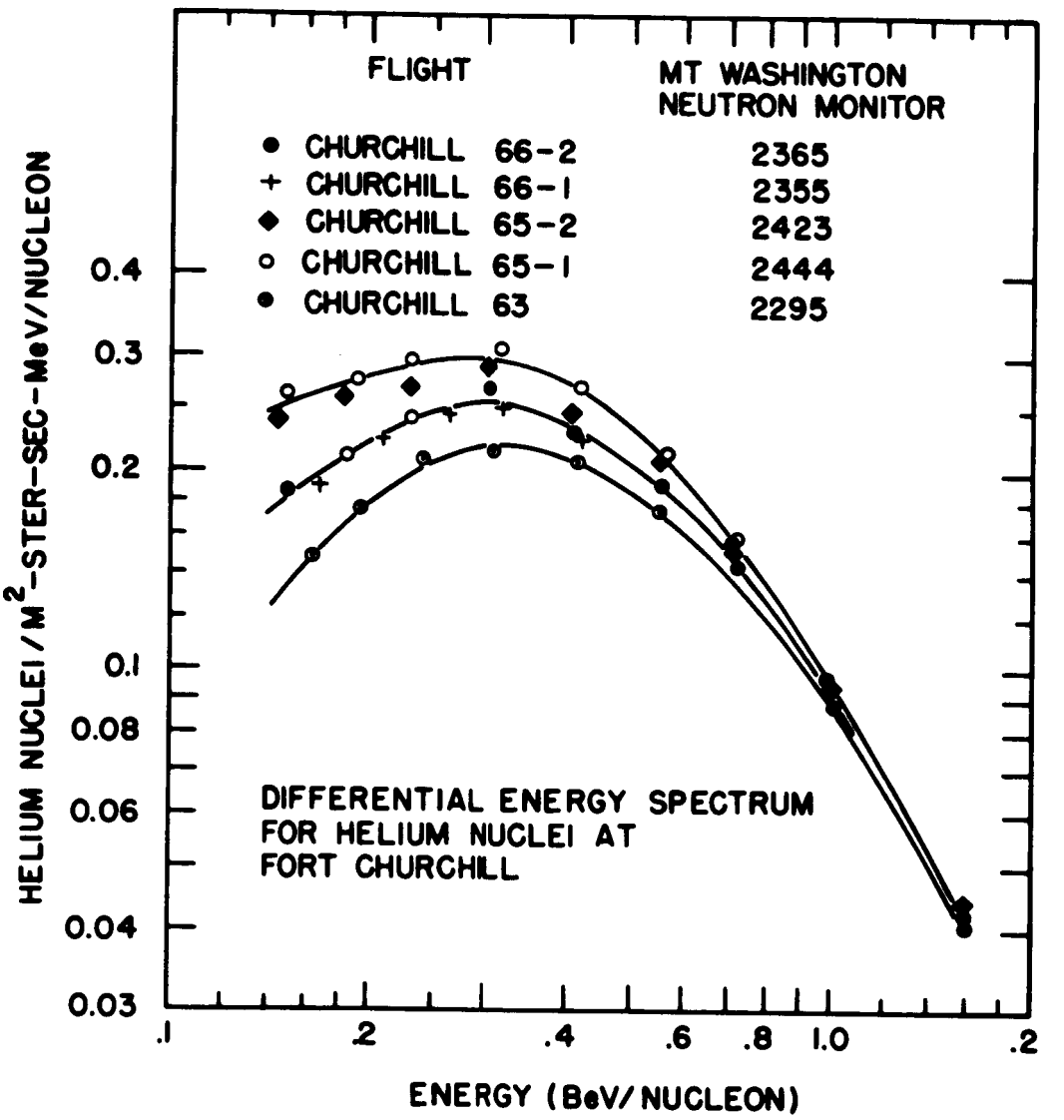
FLIGHT
MT WASHINGTON
NEUTRON MONITOR
CHURCHILL 66-2 2365
CHURCHILL 66-1 2355
CHURCHILL 65-2 2423
CHURCHILL 65-1 2444
CHURCHILL 63 2295
DIFFERENTIAL ENERGY SPECTRUM
FOR HELIUM NUCLEI AT
FORT CHURCHILL
HELIUM NUCLEI / M²-STER-SEC-MeV/NUCLEON
0.4
0.3
0.2
0.1
0.08
0.06
0.04
0.03
.1
.2
.4
.6
.8
1.0
.2
ENERGY (BeV/NUCLEON)

Figure 15

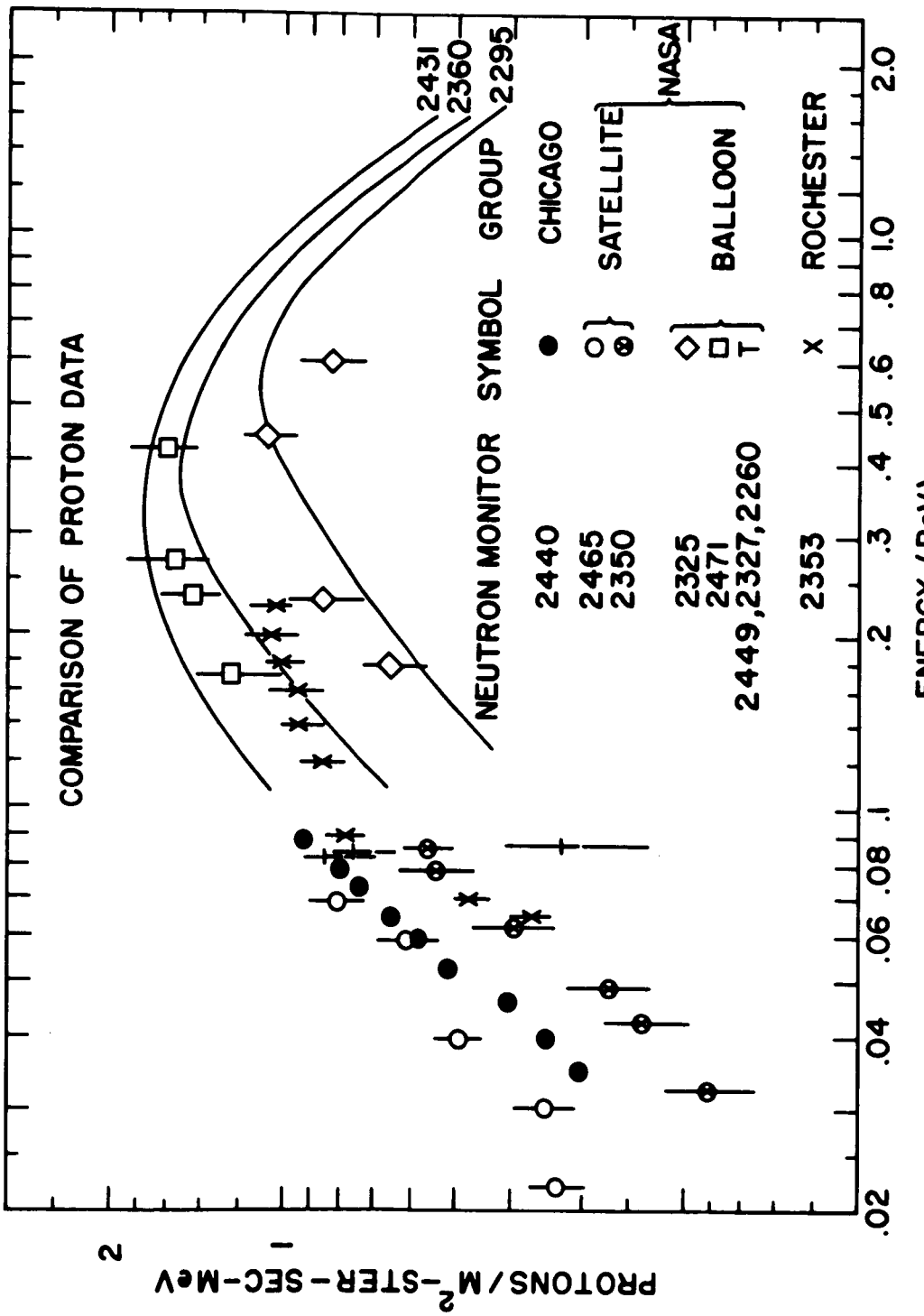
COMPARISON OF PROTON DATA
NEUTRON MONITOR SYMBOL GROUP
CHICAGO
SATELLITE
NASA
BALLOON
ROCHESTER
2440
2465
2350
2325
2471
2449,2327,2260
2353
2431
2360
2295
PROTONS/M²-STER-SEC-MeV
ENERGY (BeV)
.02
.04
.06
.08
.1
.2
.3
.4
.5
.6
.8
1.0
2.0

Figure 16

(Badhwar et al., 1967) in 1966 also agree quite well with our proton spectrum in the 100-200 MeV range.

In 1965 our spectrum matches on quite nicely again with the lower energy IMP proton data of NASA (Balasubrahmanyan et al., 1967) and also with the Chicago data from Fan et al., (1966). The proton data at higher energies from NASA balloon flights in 1965 (Balasubrahmanyan et al., 1966) falls between our 1965 and 1966 spectra. Since their flight actually corresponded to a neutron monitor rate of 2471, this data should probably lie above our highest curve. At energies above 300 MeV there is very little data of any type for comparison and none of comparable accuracy.

Turning now to the comparison of the helium nuclei measurements as presented in Figure 17, the current revisions to our 1963 data bring the differential intensities more in line with the 1963 balloon results of Balasubrahmanyan and McDonald (1964). They also agree with the results of Freier and Waddington (1965).

However, for 1965 our helium intensities fall slightly below those of Balasubrahmanyan et al., (1966), (our proton intensities are above theirs for the same day).

Both in 1963 and 1965 the low energy end of our helium spectrum falls slightly below a smooth connection to the low energy satellite data of NASA (Balasubrahmanyan et al., 1967) and Chicago (Fan et al., 1967, not shown in figure). This may be related to the slightly lower neutron monitor rates applicable for our flights or it may indicate problems associated with

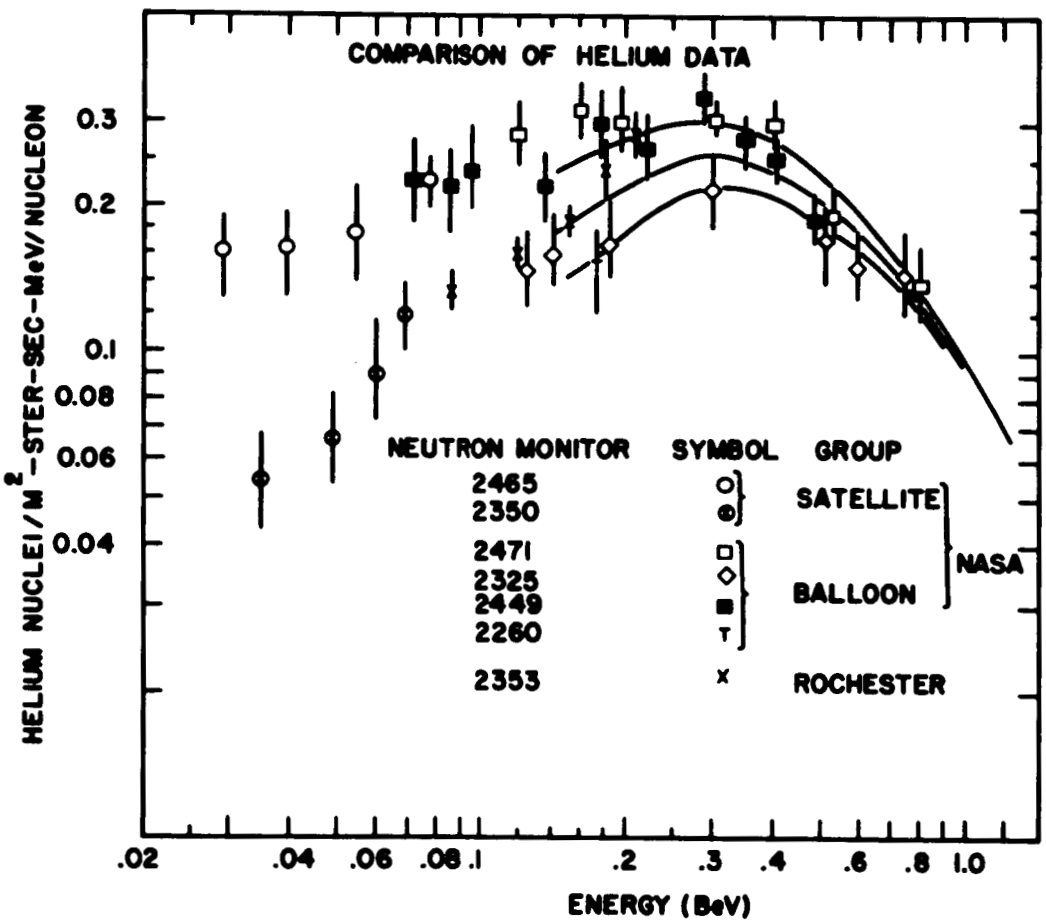
COMPARISON OF HELIUM DATA
HELIUM NUCLEI/M²-STER-SEC-MeV/NUCLEON
0.3
0.2
0.1
0.08
0.06
0.04
NEUTRON MONITOR
SYMBOL
GROUP
2465
2350
SATELLITE
2471
2325
2449
BALLOON
NASA
2260
2353
ROCHESTER
.02
.04
.06
.08
.1
.2
.3
.4
.6
.8
1.0
ENERGY (BeV)

Figure 17

determining an intensity at the limits of either or both of the balloon and satellite energy ranges. The 1966 data of the Rochester group (Badhwar et al., 1967 b) agrees quite well with our 1966 spectra except for their point at 200 MeV/nucleon which appears to be high. This is again near the upper energy limit of their dE/dx by E system.

To conclude the presentation of the spectra of protons and helium nuclei, the mean differential intensities for the cosmic ray maximum year, 1965, are presented in Table 2. These measurements were made when the neutron monitor counting rate was within 2% of its maximum value.

Table 2

Mean Differential Spectra of Protons and Helium in 1965

	Particles/m^2-ster-sec-MeV										Particles / m^2-ster-sec
Energy Range (MeV)	100–120	120–150	150–190	190–250	250–340	340–450	450–600	600–800	800–1200	1200–2000	>2000
Protons	1.05 ±.09	1.25 ±.09	1.43 ±.08	1.61 ±.09	1.72 ±.09	1.70 ±.08	1.58 ±.08	1.35 ±.07	1.00 ±.05	0.50 ±.03	1135 ± 55
Helium		0.245 ±.015	0.265 ±.015	0.285 ±.015	0.30 ±.02	0.28 ±.01	0.23 ±.01	0.163 ±.008	0.097 ±.005	0.045 ±.002	65 ± 3

V. SOLAR MODULATION THEORY

Let us turn our attention now to the modulation of the cosmic rays in the solar environment. We shall start by establishing a theoretical framework within which our data on the solar modulation can be examined.

The dominating influence in the interplanetary medium is the solar wind, that plasma which is flowing radially outward from the solar corona at velocities exceeding the Alfven velocity. Frozen into this plasma is the solar magnetic field. Due to the combined effects of the rotation of the sun (27 day period) and the outward flow of plasma, the magnetic field in the ecliptic plane assumes, on the average, the form of an Archemedian spiral with field components in polar coordinates of:

$$B_r = B_o(r_o)(r_o/r)^2, \; B\phi = -\Omega r B_r/V$$

Here $B_o(r_o)$ is the field at the reference point r_o, Ω is the angular velocity of the sun and V is the solar wind velocity. As early as 1956 Parker (1956) anticipated our present knowledge and linked the modulation of cosmic rays to the sweeping out effect resulting from the scattering of cosmic rays from magnetic irregularities superimposed on this average field.

In Parker's picture the dominant process is one in which the particles are convected out of the solar system by the "frictional drag" resulting from their collisions with the magnetic scattering centers flowing outward in the solar wind.

This process competes with a diffusion of cosmic rays through this region of scattering centers. Under steady state conditions this simple diffusion-convection picture is represented by the following equation.

$$\vec{\nabla} \cdot \left[\vec{V}\, n(\vec{r},R)\right] = \vec{\nabla} \cdot \left[\, D\, \vec{\nabla}\, n(\vec{r},R)\right] \qquad (7)$$

$\vec{V}$ is the transport velocity of the magnetic irregularities (the solar wind velocity), D is the diffusion coefficient, n is the particle density, and R is the rigidity.

Many authors (Skadron, 1967 and Axford, 1965) have attempted to include the effects of energy loss in their treatment of the modulation problem. Effects such as adiabatic deceleration, inverse Fermi deceleration and possible deceleration effects due to electric polarization ($\vec{V} \times \vec{B}$) fields will not be considered in this discussion.

Let us consider equation (7). The particle density n is dependent upon heliocentric radius, r, and upon particle energy and charge. The diffusion coefficient is given by:

$$D = 1/3\ \lambda(\vec{r},R)\vec{v} \qquad (8)$$

Here λ, the mean distance in which a particle traveling with velocity $\vec{v}$ loses all memory of its original direction, is known as the scattering mean free path. In general λ is a tensor which may be represented by a component parallel, $\lambda_{\parallel}$ and a component perpendicular, $\lambda_{\perp}$, to the local magnetic field. This mean free path (and hence D) depends on r and also on the rigidity R of the particle.

Since diffusion along the field is so much easier than diffusion across field we may assume that one dimensional diffusion along the field lines dominates, as suggested by Jokipii (1966) and Lietti and Quenby (1967). Equation (7) can then be simplified and integrated to give

$$n(r,R) = n(r_b,R) \exp \left[3V/v \int_r^{r_b} \frac{dr}{\lambda(r,R)} \right] \qquad (9)$$

where r_b is the radius of the boundary of the modulating region or more properly the arclength along the Archimedean spiral of the average solar magnetic field.

In order to solve the modulation problem, the dependence of λ on the spatial coordinate r and on rigidity R must be determined. Let us assume that this dependence on r and R is separable and turn our attention to the rigidity term. Dorman (1963) first recognized that a particle would be scattered quite differently by magnetic inhomogeneities of different wavelengths. This idea has recently been expanded upon by both Roelof (1966, in conjunction with solar particles) and Jokipii (1966). They considered a whole spectrum of irregularity sizes (wavelengths), and using statistical techniques found that those comparable in size to the Larmor radius of the particle in the average field were the most effective for producing large angle scattering.

In this formulation of the problem the dependence of λ_{11} on rigidity is determined to be

$$\lambda_{11} = R^2/M(K) \qquad (10)$$

where M(K) is the power spectrum (in wave numbers, K) of magnetic

irregularities. The power spectrum can be written

$$M(K) \propto 1/K^{\gamma} \tag{11}$$

Replacing the radius of curvature by the corresponding rigidity and combining equations (10) and (11) we obtain:

$$\lambda_{11} \propto R^2/R^{\gamma} \tag{12}$$

The power spectrum of the magnetic field irregularities has recently been measured by Coleman (1966) and Ness et al., (1966 a,b). The exponent γ of this spectrum appears to be 1.0 for irregularity wavelengths between 0.002 AU. and 0.06 AU., possibly steepening at smaller wavelengths. This corresponds to rigidities from 0.3 to 10 BV in the average interplanetary field of 5×10^{-5} gauss near 1 AU. The important feature to be stressed here is that while the measured power spectra have been obtained near the earth, the cosmic rays are certainly modulated over a much larger region. It is by no means certain that the exponent of the power spectrum will remain constant over this region, the radius of which may be anywhere from 5 to 50 AU. If the above theoretical picture is correct, however, we can use an accurate measurement of the rigidity dependence of the modulation of cosmic rays to determine the average power spectrum of magnetic inhomogenieties over the whole modulating region.

The power contained in the magnetic irregularities quite probably depends upon r. This coupled with the unknown radial dependence of γ makes the theoretical situation with

is perhaps "in agreement" with the experimental situation since there appears to be a wide divergence of experimental results (as pointed out by O'Gallagher and Simpson, 1967).

The problem of the interplanetary cosmic ray gradient is crucial in "demodulating" the cosmic ray spectrum to determine $n(r_b,R)$, the density outside of the solar system. Recent attempts (Durgaprasad et al., 1967) in this direction have met with somewhat limited success. We shall not deal with this problem here. Our principal concern will be with the rigidity dependence of the modulation as measured at the earth.

Inserting the mean free path from equation (12) into equation (9) one obtains:

$$n(r,R) = n(r_b,R) \exp \frac{-3VA(r)}{\beta c R^{2-\gamma}} \qquad (13)$$

$A(r)$ includes the proportionality constants and the integral involving the radial dependence which was written out specifically in equation (9). Here V and A are certainly time dependent, and γ may also depend upon time.

The measurements to be considered here have been made at $r = r_e$, but at different times. Rewriting the above equation combining the time dependence and the constant factors into the single term $\eta(t)$ we get

$$n(t,R) = n(r_b,R) \exp \frac{\eta(t)}{\beta R^{2-\gamma}} \qquad (14)$$

Experimentally we compare the differential spectrum dj/dE at two times. Assuming that the cosmic ray intensity is isotropic and taking logarithms of both sides we obtain

$$\beta \ln \left\{ \frac{dj/dE\ (t_1,E)}{dj/dE\ (t_2,E)} \right\} = \frac{\eta(t_1) - \eta(t_2)}{R^{2-\gamma}} \equiv \frac{\Delta\eta}{R^{\alpha}} \qquad (15)$$

where the quantity on the left is directly measured.

This expression for the functional form of the modulation is particularly appealing to the experimentalist because of its simplicity. All of the information about the scattering irregularities is contained in the single parameter γ which can be examined as a function of time and rigidity.

Equation (15) conveniently separates into a velocity dependent term on the left and a rigidity dependent term on the right. If the experimentally determined left hand side of equation (15) is plotted as a function of rigidity, protons and helium nuclei should look the same independent of the value of the exponent γ. Furthermore if the modulation is independent of rigidity, the data should fall on a straight line with zero slope.

VI. MEASUREMENTS OF THE MODULATION

We shall now proceed to our direct measurements of the modulation and attempt to combine these results with those of other workers to obtain an overall look at the rigidity dependence of the modulation process. The following word of caution should be injected, however. While our intention has been to study the long term (11 year) modulation of cosmic rays, it is possible that the short term modulations, which are included in our measurements, may be significant. It is not certain that both the long term and shorter term modulations have the same functional form, although no good evidence has been found to the contrary. The assumption will be made that this study is of a single phenomenon only, and not a superposition of several different ones.

In Figure 18 the data on the modulation of protons and helium nuclei as measured by our telescope is presented. On the ordinate is plotted

$$\beta \ln \left\{ \frac{dJ/dE\ (1965,\ E)}{dJ/dE\ (63 \text{ or } 66,\ E)} \right\} \qquad (16)$$

and on the abscissa is plotted the rigidity of the particle. The slope derived from this figure leads directly to a determination of the exponent $\alpha = 2-\gamma$ and hence to γ itself. This type of plot has been suggested by Jokipii (1967).

In this figure our data is compared with the change in the Mt. Washington neutron monitor rate which is shown plotted at

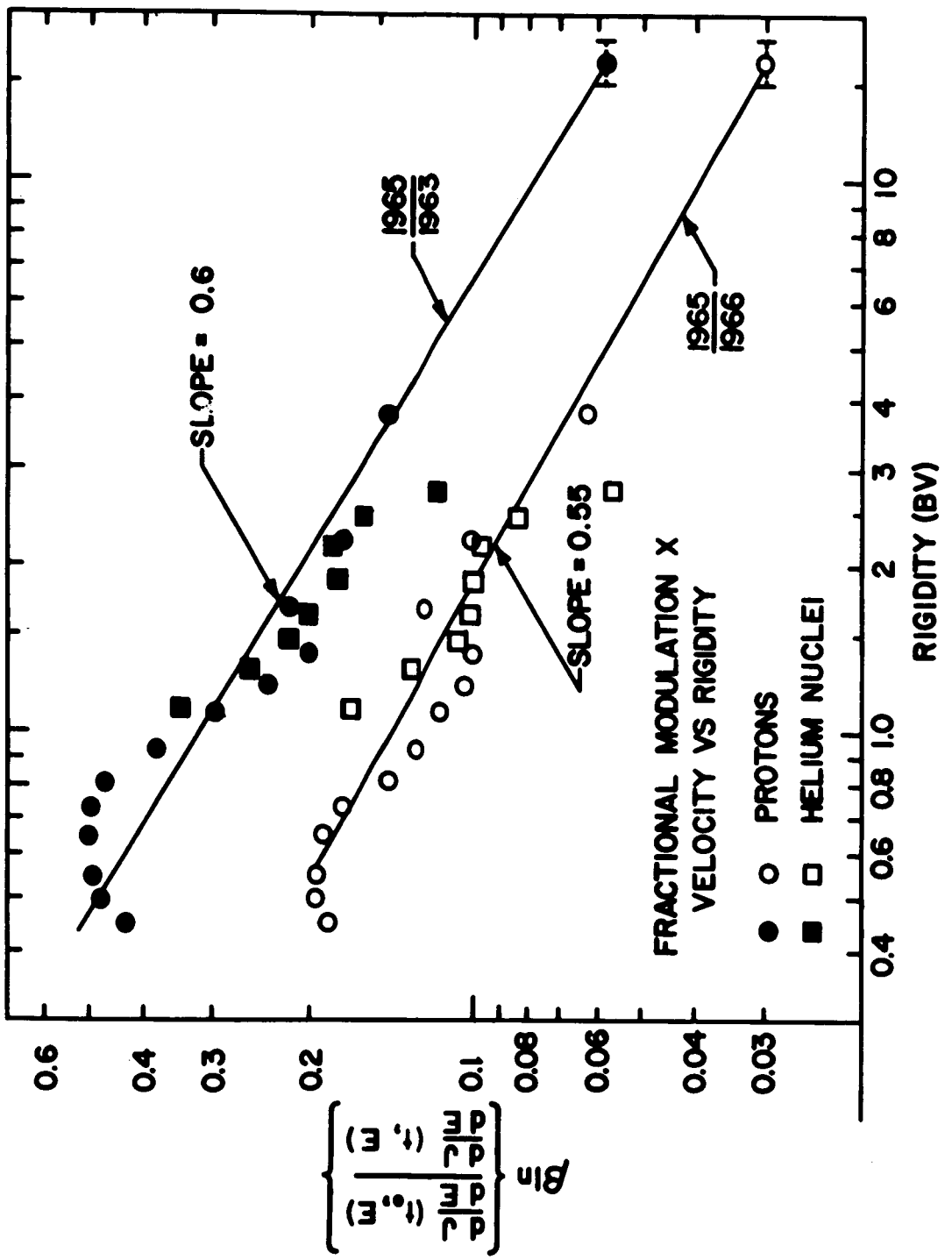
SLOPE = 0.6
1965/1963
1965/1966
SLOPE = 0.55
FRACTIONAL MODULATION X
VELOCITY VS RIGIDITY
PROTONS
HELIUM NUCLEI
RIGIDITY (BV)
0.4
0.6
0.8
1.0
2
3
4
6
8
10
0.6
0.4
0.3
0.2
0.1
0.08
0.06
0.04
0.03

Figure 18

an "effective" rigidity 15-18 BV. This is the rigidity of the mean response of the Mt. Washington monitor to a $1/\beta R^{\alpha}$ modulation at sunspot minimum for $\alpha \simeq .5$, calculated using the yield functions recently presented (Lockwood and Webber, 1967). At periods of greater modulation, the cosmic ray spectrum becomes harder (relatively more high energy particles) raising this mean response rigidity somewhat. However, the exponent α appears to increase slightly which tends to lower the mean response rigidity, and so we plot the neutron monitor data at a rigidity of 15-18 BV for all modulation epochs.

The exponent in the rigidity dependence is 0.55 and 0.6 for our measurements in 1966 and 1963 respectively. This suggests that the effective exponent in the spectrum of magnetic irregularities is 1.45 near sunspot minimum perhaps decreasing slightly with increasing solar modulation. While this difference between the exponents in the two years is hardly significant, we can definitely say that in this energy range, the modulation we measure is neither simply of the form $1/\beta$ nor the form $1/\beta R$ but lies almsot half way between.

Recall our earlier observation that the integral intensity of protons above 450 MeV/nucleon had changed by 1.5 times as much as the integral intensity of helium nuclei at the same energy. We find that this observation is quite compatible with an exponent α between 0 and 1. If the exponent were 0 (the form of the modulation was $1/\beta$) then at the same energy/nucleon the protons and alphas would have the same modulation. If the exponent were 1

and the modulation form was $1/\beta R$ then at the same energy/nucleon the protons would be modulated twice as much as helium. The measured modulation ratio of 1.5 implies an exponent $\simeq .5$.

While our conclusions on the functional form of the modulation are somewhat different from those drawn previously by other workers, they are not inconsistent. This is because most workers have not, in fact, been able to discriminate between a $1/\beta$ and $1/\beta R$ dependence (eg. see Silberberg, 1966 or Badhwar et al., 1967).

In an attempt to extend this data over a greater energy range and over a larger part of the solar cycle, we have taken the compilation of data in the recent review of Webber (1967) and converted it to the type of plot on which this data has been presented. This is shown in Figure 19. All modulations are measured with respect to our 1965 data.

The first feature we wish to point out is that all the pre 1963 data at the lowest energies is consistent with a purely velocity dependent modulation. Because the amount of modulation at rigidities to which the neutron monitor is sensitive is clearly much less than at lower energies, there must be some transition at which a rigidity dependence enters the modulation. This is shown as a sharp break in the curves connecting the high and low rigidity regions. The modulation at higher rigidities is represented by connecting these break points to the neutron monitor values with straight lines.

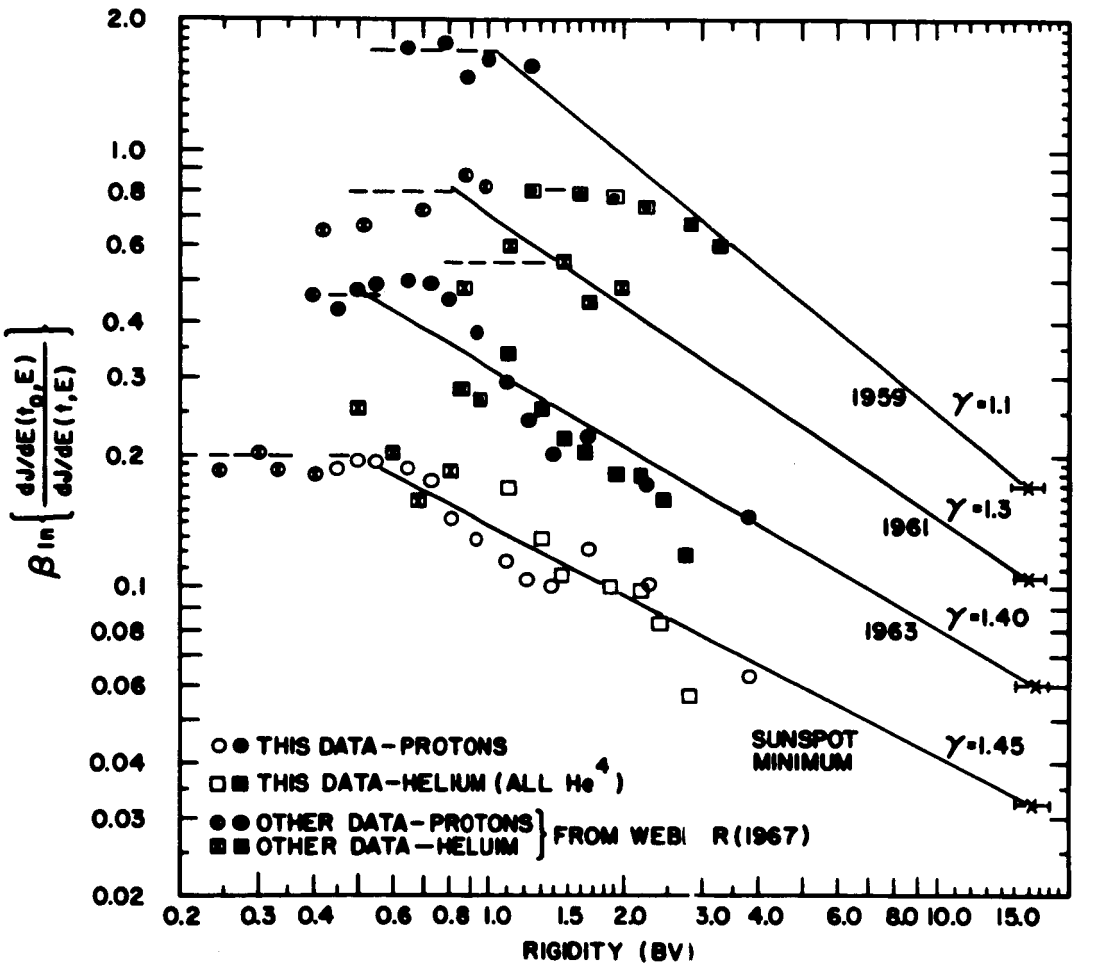
2.0
1.0
0.8
0.6
0.4
0.3
0.2
0.1
0.08
0.06
0.04
0.03
0.02
$\beta \ln\left\{\frac{dJ/dE(T_0,E)}{dJ/dE(T,E)}\right\}$
1959
γ=1.1
1961
γ=1.3
1963
γ=1.40
γ=1.45
SUNSPOT MINIMUM
THIS DATA-PROTONS
THIS DATA-HELIUM (ALL He^4)
OTHER DATA-PROTONS
OTHER DATA-HELIUM
FROM WEBI R(1967)
0.2 0.3 0.4 0.6 0.8 1.0 1.5 2.0 3.0 4.0 6.0 8.0 10.0 15.0
RIGIDITY (BV)

Figure 19

At rigidities above this break the results for the four different epochs of modulation give values of γ which decrease with increasing solar activity. This implies that the power spectrum of magnetic inhomogenity sizes is getting flatter with decreasing solar activity, ie. the longer wavelengths are increasing in importance relative to the shorter ones. It must be emphasized that, if this picture is correct, γ represents the mean exponent of the spectrum of magnetic irregularity wavelengths seen by the cosmic rays over the whole modulating region. Since the measurements near the earth's orbit (Coleman, 1966, and Ness et al., 1966 a,b) indicate exponents nearer 1, we suggest that the power spectrum of the magnetic irregularities might be modified in shape becoming steeper as one moves away from the sun.

Consider now the question of a simple velocity dependent modulation at low energies as evidenced by the data in Figure 19. The most reliable data which presents clear evidence for a flat portion in these curves is the low energy proton data below 0.6 BV from the NASA group taken at times near sunspot minimum. However at this same time, the helium data at the same velocity still shows rigidity dependent modulation. This data is taken with the same satellite borne detector. Hence at the same rigidity (when $R \leq 0.7$ BV) helium appears to be modulated more than protons. However in 1959, at low energies protons were being modulated twice as much as helium at the same rigidity. A similar feature was noted by Webber (1967) in his recent review.

In this plot, a changeover from a $1/\beta R^{\alpha}$ dependence to a $1/\beta$ dependence is reflected in a flattening of the curves shown in Figure 19. For protons, the rigidity (or velocity) at which the changeover (break) from $1/\beta \rightarrow 1/\beta R^{\alpha}$ occurs appears to depend on the level of solar modulation, increasing from about 0.5 BV to about 1 BV with increasing solar modulation. The changeover point for helium nuclei however has increased from $\leq$ 0.5 BV to $\simeq$ 2. BV during the same period, or twice as much change as for protons. This is one way of describing the peculiar proton to helium modulation discussed in the previous paragraph.

This behavior of the relative modulation of protons and helium nuclei is very difficult to understand. It appears to have no simple explanation within the framework of the model we have been discussing. If the changeover were to be interpreted as an abrupt change in the power spectrum of magnetic inhomogeneities it should occur at the same rigidity for protons and helium nuclei at all times in the solar cycle, even if that rigidity itself were to change. This clearly does not appear to be happening. On the other hand if the changeover in the form of the modulation were due to the increased importance of energy dependent processes, the changeover rigidities should differ by a factor of 2 throughout the solar cycle. This does not appear to be happening either.

The data we have presented and summarized gives strong evidence of changes in the rigidity dependence of the modulation that cannot be represented in a simple manner. Only near sunspot minimum has sufficient data been available to experimentally

define the functional form of the modulation. It is hoped that the equipment described in this paper can be flown periodically throughout the remainder of the current cycle, for it appears that it is in the range of the greatest sensitivity of this instrument, from 0.4 BV to 4 BV rigidity, that important and not well understood (or defined) changes in the functional form of the modulation occur.

APPENDIX 1

TELESCOPE RESPONSE CHARACTERISTICS

a.) Calculated Response Curves

The three dimensional nature of the response of the telescope is expressed in Figure 2 of the main text as S_t vs S + C, and in Figures A-1 and A-2 which show S_m vs S + C and S_t vs S_m respectively.

The two modes of the telescope S_t vs S + C and S_m vs S + C are essentially similar. The principle difference is that the S_t vs S + C mode has 0.7 gm/cm^2 of absorber between the two detection elements while there is no absorber between the two elements in the S_m vs S + C mode. The effect of this matter can be seen in the response to the low energy protons.

Another feature of the two scintillator vs S + C modes is that they are effectively beneath different amounts of "atmosphere" because the S_m vs S + C mode looks through the S_t element, whereas the S_t vs S + C mode looks only at the overlying atmosphere. This means the low energy secondary protons generated above the telescope can be examined at two separate depths.

The two modes also have different background properties arising from the difference in matter between detectors. Particles which interact in S_t produce products which are absorbed in S_m, the net result being a small pulse in the S + C element. However, when an interaction takes place in S_m there is less absorption of the products before they reach the S + C element. The result is

that in the S_t vs S + C distributions, the background tends to be concentrated at low values of S + C while in the S_m vs S + C distributions the background is distributed more uniformly over all values of S + C.

The most obvious advantage of having two ionization loss measurements is that they can be directly compared for consistency. The method of selecting the consistency requirements is suggested in the response curve for the third mode of the telescope, S_t vs S_m shown in Figure A-2. The response for all particles which can penetrate S_m lies close to the diagonal. Two methods of requiring consistency are as follows:

$$|S_t - S_m| < |S_t + S_m| \; k_1 \qquad \text{(A-1)}$$

$$|S_t - S_m| < k_2 \qquad \text{(A-2)}$$

Either or both requirements may be utilized with various constants.

The penetration counter has two valuable features. It removes from the distribution a large flux of electrons which are incapable of penetrating more than 10 gm/cm^2 but which otherwise look just like minimum ionizing protons. Secondly, it removes the ambiguity which occurs when the low energy proton response crosses the helium response. This is particularly necessary in the S_m vs S + C mode as can be seen in Figure A-1.

b.) Sample Pulse Height Distributions

The features of the different modes of response of this telescope which have been described above are demonstrated in

Figures A-3 through A-11.*

Figure A-3 shows the relativistic proton and helium peaks on an exponential alphameric S_t vs S + C, P distribution. A factor of 2 reduction in resolution over the maximum attainable has been made, and hence this is called a 2:1 distribution. The relativistic proton peak is seen at 22 by 15 and the relativistic helium peak is at 116 by 64. The spectrum of helium can be seen unfolding to the left and downward.

This distribution should be compared with the S_t vs S + C, $\bar{P}$, 2:1 distribution in Figure A-4. The non-penetrating electrons which have been separated from the proton peak can now be seen at S_t = 22. Note also the clear absence of counts in the region of the helium peak, 116 by 64.

The next four figures show in 1:1 scale the energy region just below the helium nuclei Cerenkov threshold (320 MeV/nucleon) for the following four cases: Figure A-5, S_t vs S + C, P; A-6, S_t vs S + C, $\bar{P}$; A-7, S_m vs S + C, P; and A-8, S_m vs S + C, $\bar{P}$.

Comparing A-5 and A-7, note that the background events are more concentrated near S + C equal zero in the S_t distributions and are more generally spread out in the S_m distributions. Both these distributions show helium nuclei between 160 and 320 MeV/nucleon. In Figures A-6 and A-8 note that for S_t distributions the low energy protons barely reach this range of pulse heights

*In these distributions, there are two types of scale used. In the "exponential alphameric" distributions, the numbers shown represent x where $2^x \leq N < 2^{x-1}$. N is the number of counts in the cell. Counting begins with the numbers 0,1,2... and continues with the alphabet, so that an A=10 represents an N as follows: $1024 \leq N < 2048$. In the "linear alphameric" outputs N itself is shown, with the counting proceeding A=10, B=11, etc.

(7.5 to 11 times minimum) whereas in the S_m distribution the low energy protons are very well defined at these pulse heights.

In Figure A-9 the manner in which the consistency requirement is imposed on the two pulse heights S_t and S_m is shown. This is a 2:1 scale S_t vs S_m, P distribution. The constant in Formula A-2, chosen here to be $k_2 = 32$, requires that the particles lie between the two lines shown. The result of the application of this selection is shown in Figures A-10 and A-11.

The selected distribution shown in Figure A-10 is exactly the same as the unselected one shown in A-3, namely S_t vs S + C, P, 2:1 scale. Note how the background has been removed. This is even more dramatically shown in A-11 which is the same as A-5. In these two S_t distributions one can easily see that the background concentrated at S + C near zero is removed by the selection process.

APPENDIX 2

PULSE HEIGHT DISTRIBUTIONS TO SPECTRA

a.) Reduction of the Two Dimensional Pulse Height Distributions

In the main body of the text the convolution of the Symon energy loss distributions with Gaussian distributions (representing the intrinsic detector response) is discussed. The purpose of this convolution is to obtain the composite response functions R(E,x). It represents the distribution of fluctuations in pulse height x which may be suffered by a particle of energy E.

The measured quantity from a detector is a differential pulse height distribution dM(x)/dx. This is related to the differential energy spectrum dj(E)/dE incident upon the top of the telescope through the following equation:

$$\frac{dM(x)}{dx} = \int_0^\infty R(E,x)\,\frac{dj(E)}{dE}\,dE$$

In order to derive the energy spectrum from the measured two dimensional pulse height distributions this equation must first be reduced to a more tractable form. We replace it by the set of linear equations

$$M_j = \sum_j S_j\, r_{ij}$$

where S_j is the spectral number of counts in the jth energy bin, M_i is the measured counts in the ith bin, and r_{ij} is the fractional area of the response curve for the jth interval $R(E_j,x)\,\Delta x_i$ lying in the ith interval. The pulse height scale

is divided into the 10 intervals bounded by the energies 2000, 1200, 800, 600, 450, 340, 250, 190, 150, and 120 MeV, in the S_t (or S_m) dimension. This subdivides one of the dimensions, and the solution to the linear system will correct for the fact that a particle undergoing a fluctuation in this dimension will appear at a new point on the energy scale.

Because of the two dimensional nature of the distributions some simplification can be made to the above set of coupled equations. It is accomplished by utilizing the energy variation of output from the S + C detector to partially decouple the system of ten equations. The fact that the S + C intervals (the range of S + C pulse heights allowed for a given value of S) do not lie directly beneath one another is thusly taken into account.

To examine this in more detail, we begin by considering an event in pulse height interval i on the S axis. For this interval a certain range of S + C pulse heights is allowed, say $y_i \pm \Delta y_i$ where Δy_i is determined by the half points (same as FWHM) on the S + C distribution at energy i. (Where Δy cannot be directly determined from the pulse height distributions, the variation in S + C interval size is obtained by assuming that the S + C light output is dominated by photoelectron statistics with a slight adjustment for the varying resolution of the Symon distributions with energy.) Suppose a particle in pulse height bin i fluctuates and lands in the pulse height bin j. In the S + C dimension the particle will still lie in

the range $y_i \pm \Delta y_i$ since the particle response in this detector is independent of the fluctuation which took place above. Now bin j will include a range of pulse heights $y_j \pm \Delta y_j$ in the S + C dimension, some of which may overlap the range $y_i \pm \Delta y_i$. The fraction of this overlap (weighted by the S + C distribution function) represents the efficiency with which the interval i is connected to j in the S + C dimension. This gives rise to a set of decoupling coefficients which depend upon the resolution and on the S/C ratio of the S + C detector. The coefficients are smaller (better decoupling) for better resolution and for lower S/C ratios.

Call these decoupling coefficients d_{ij}. The coefficient d_{ij} then represents the probability that an event, which belongs to the ith spectral bin and fluctates into the jth measured bin, will actually lie in the jth bin in the S + C dimension (all $d_{ii} = 1$).

The equation to be solved then becomes

$$M_i = \sum_j S_j \, r_{ij} \, d_{ij} = \sum_j S_j \, P_{ij}$$

It was originally hoped that this matrix of P_{ij}'s could be inverted and the S_j's found directly, but this proved impossible. This can be demonstrated by Figure A-12. This figure shows the various matrices for the first Churchill flight in 1966. They are respectively from top to bottom r_{ij}, d_{ij}, P_{ij} and $(P_{ij})^{-1}$. Because of the alternating signs in $(P_{ij})^{-1}$, a 1% error in the ratio of M_3/M_4, for example, would produce a 10% error in the

ratio of S_3/S_4. This enhancement of errors proved to be too large to be tolerated and so the method finally used to solve the system of ten equations is an iterative procedure whereby the S_j's are guessed, put into the above equation, and the M_i's determined. The object is to then adjust the S_j's until the measured M_i's can be reproduced within statistical errors, consistent with smooth spectra of the S_j's.

This technique is used from 2 BeV down to 120 MeV at which energy the $S_j \simeq M_j$ because the energy interval widths have become comparable with the FWHM's of the distributions.

b.) Quality of Symon Distributions

Still to be considered is whether or not Symon distributions, which represent the actual fluctuations in energy loss of a particle to a quite good degree (Gooding and Eisberg, 1957), represent the actual fluctuations to be expected in light output from the detector.

Symon's (1948) distributions include the probability that the particles will undergo large fluctuations in energy loss. These fluctuations are most pronounced (see Figure 4) for minimum ionizing singly charged particles with $\beta \simeq 1$. The integral distribution (which corresponds to the differential Symon distribution shown in Figure 4) tells us that there is a 10% probability of a fluctuation occurring with an energy loss greater than 1.7 times the most probable energy loss. This arises because of the production of one or more high energy knock-on electrons. In fact this knock-on electron, when produced, must have energy of the order of E_p giving it

a range comparable to the thickness of the detector itself. Thus the chance is relatively high that this knock-on electron will leave the detector element reducing the energy deposited in the crystal.

This effect has been considered by Lund and Risbo (1965) who have performed a Monte Carlo calculation to determine where the electron is produced in the crystal, what its angle of emergence is, and what distributions should be expected in light output. Their work indicates that for a crystal of about 1.2 gm/cm^2 thickness, there should be no fluctuations beyond a pulse of twice the most probable light output, $2\ L_p$, for a minimum ionizing particle. For lower energy incident particles, the energy loss transported outside of the crystal goes to zero because the maximum transferable energy is proportional to $\beta^2/(1-\beta^2)$. To correct for this phenomenon we require that our Symon distributions tend smoothly to zero at $2\ L_p$. Allowing the "real" Symon distributions to extend beyond $2\ L_p$ gives totally unreasonably results in the low energy part of the spectrum.

LIST OF APPENDIX FIGURES

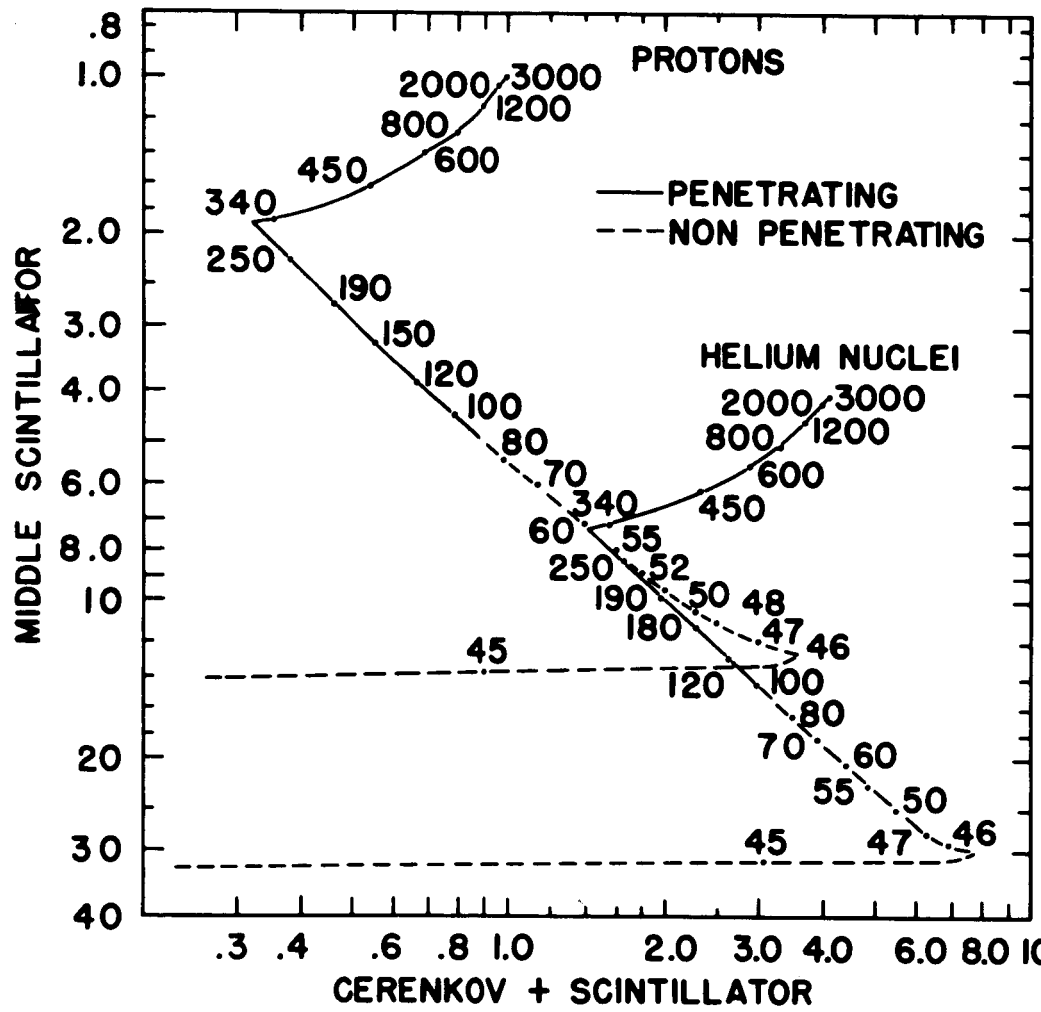
PROTONS
PENETRATING
NON PENETRATING
HELIUM NUCLEI
MIDDLE SCINTILLATOR
CERENKOV + SCINTILLATOR
.8
1.0
2.0
3.0
4.0
6.0
8.0
10
20
30
40
.3
.4
.6
.8
1.0
2.0
3.0
4.0
6.0
8.0
10
2000
3000
1200
800
600
450
340
250
190
150
120
100
80
70
60
55
52
50
48
47
46
45

Figure A-1

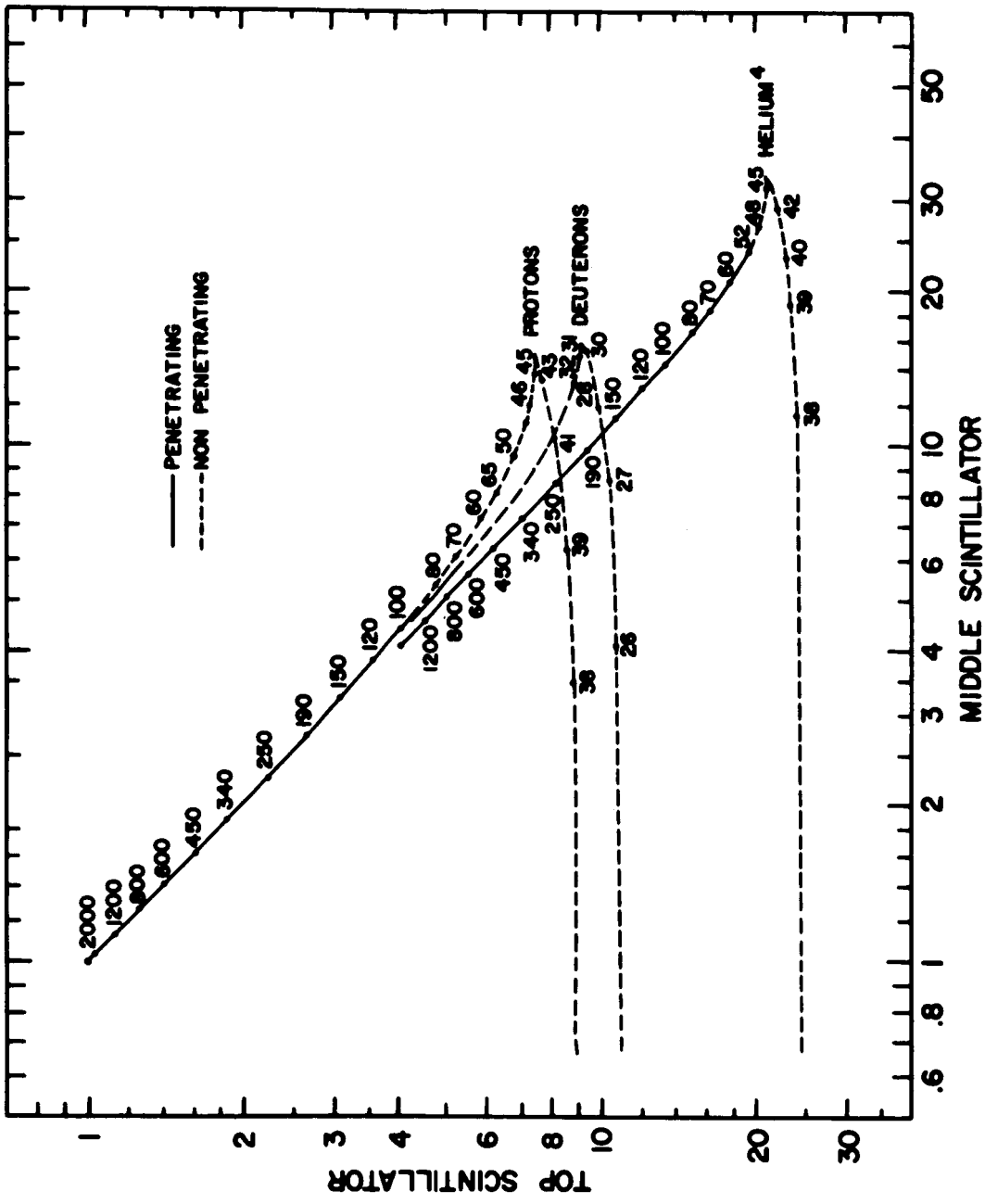
PENETRATING
NON PENETRATING
PROTONS
DEUTERONS
HELIUM⁴
TOP SCINTILLATOR
MIDDLE SCINTILLATOR

Figure A-2

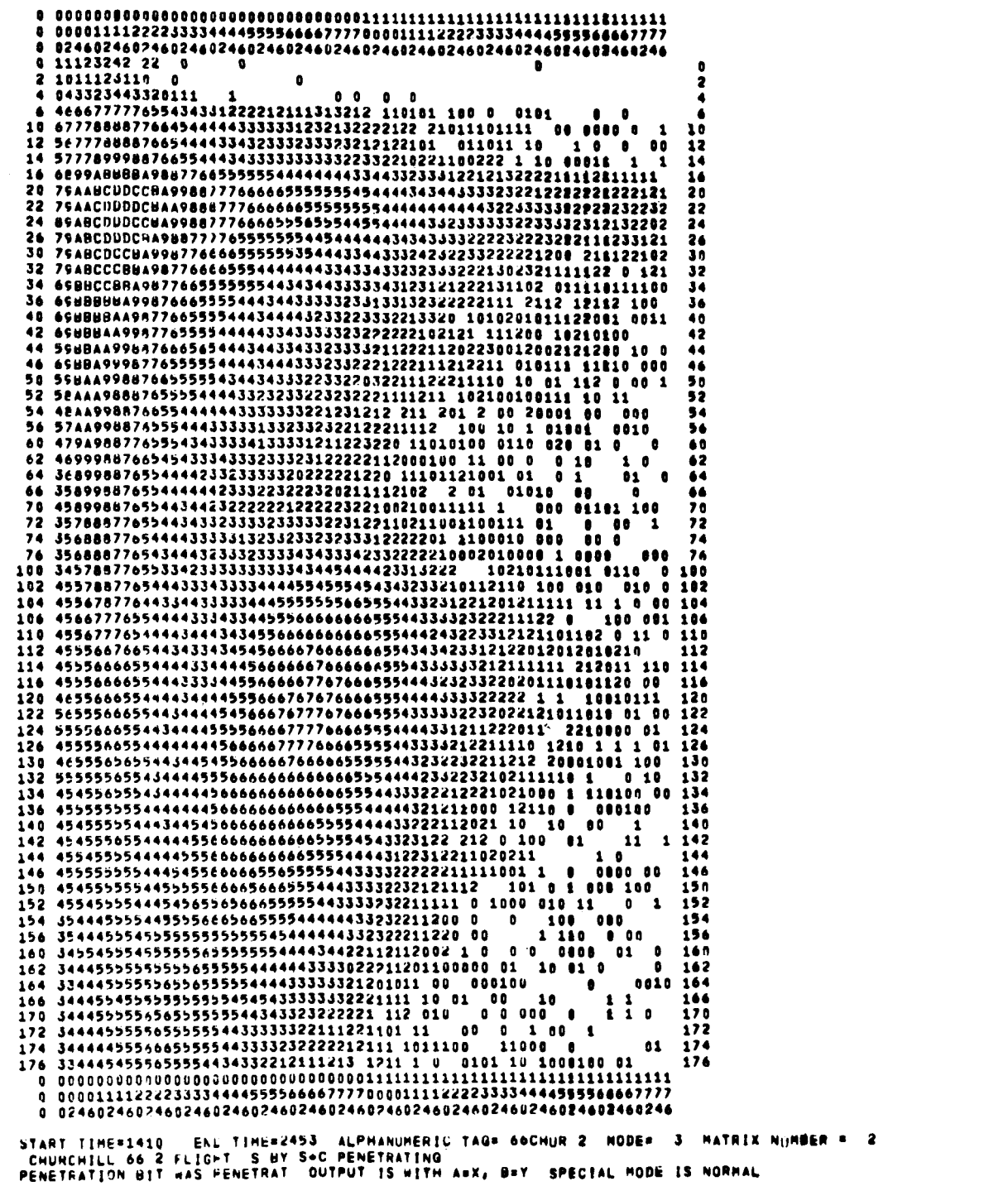
EXPONENTIAL ALPHAMERIC OUTPUT
START TIME=1410 END TIME=2453 ALPHANUMERIC TAG= 66CHUR 2 NODE= 3 MATRIX NUMBER = 2
CHURCHILL 66 2 FLIGHT S BY S=C PENETRATING
PENETRATION BIT WAS PENETRAT OUTPUT IS WITH A=X, B=Y SPECIAL MODE IS NORMAL

Figure A-3

EXPONENTIAL ALPHAMERIC OUTPUT

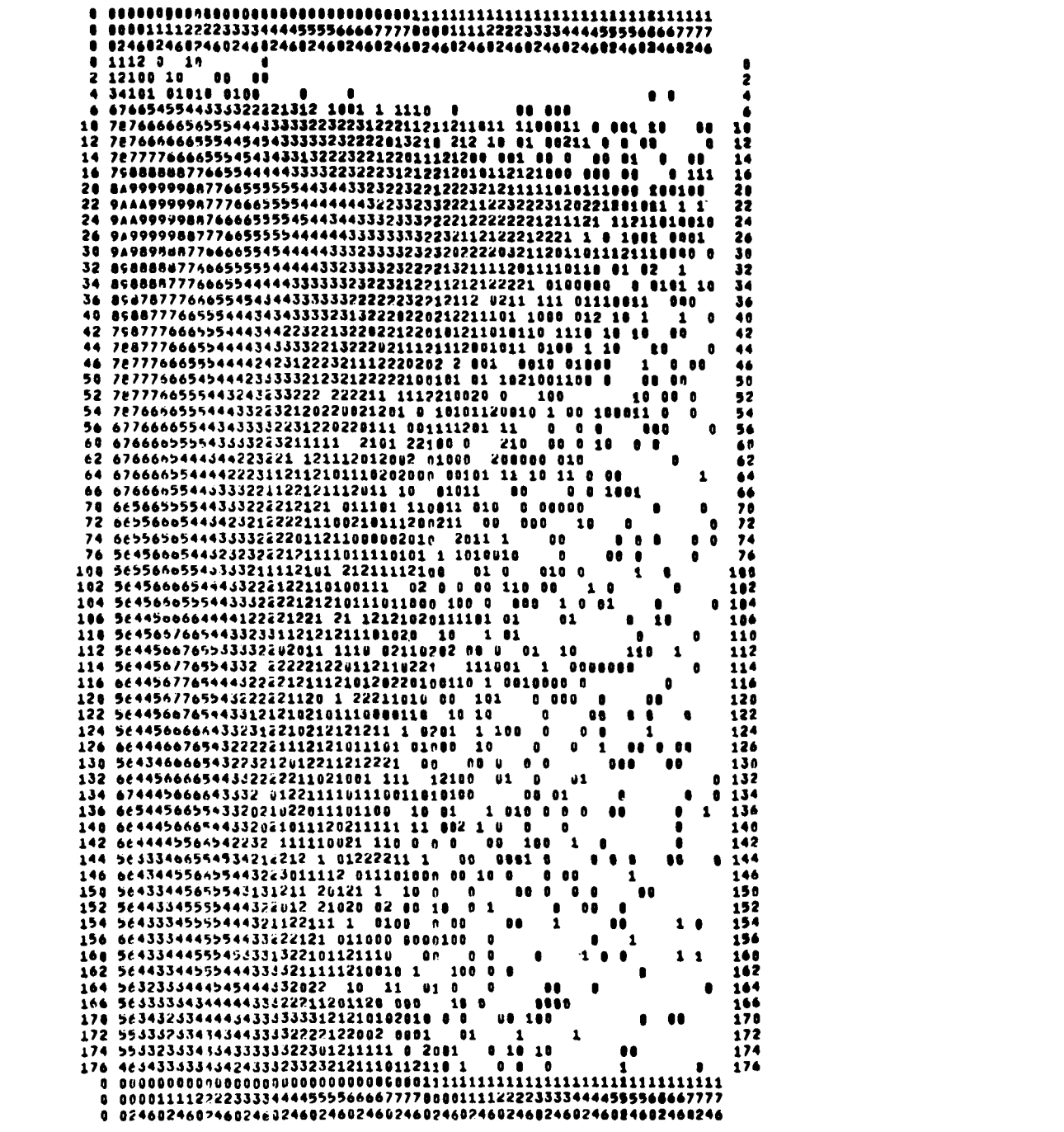

START TIME=1410 END TIME=2453 ALPHANUMERIC TAG= 66CHUN 2 MODE= 3 MATRIX NUMBER = 2
 CHUNCHILL 66 2 FLIGHT S BY S-C NOT PENETRATING
PENETRATION BIT WAS NOT PENT OUTPUT IS WITH A=X, B=Y SPECIAL MODE IS NORMAL

Figure A-4

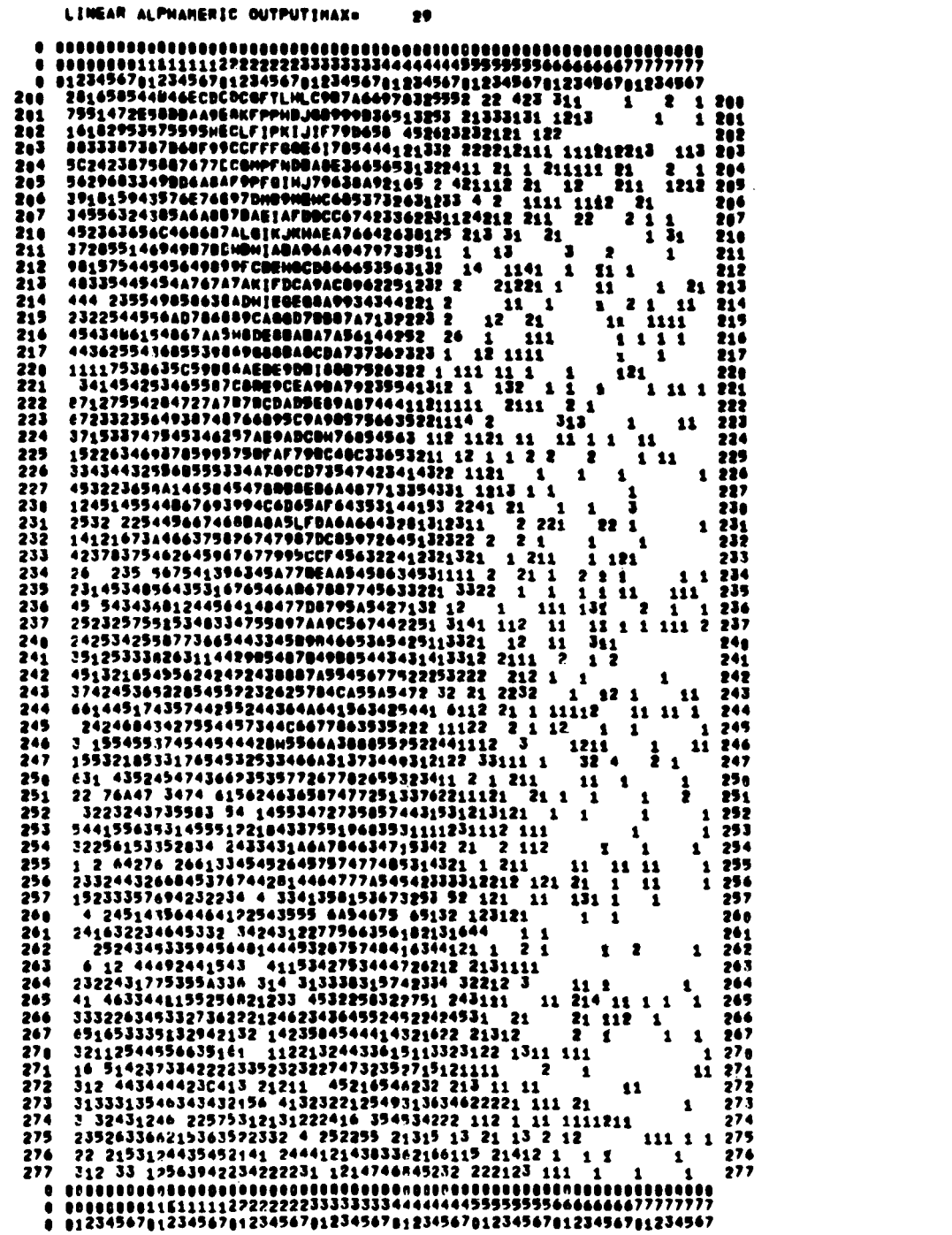
LINEAR ALPHANUMERIC OUTPUTIMAX= 89
START TIME=1418 END TIME=2453 ALPHANUMERIC TAG= 66CHUR 2 MODE= 3 MATRIX NUMBER = 7
PENETRATION BIT WAS PENETRAT OUTPUT IS WITH A=X, B=Y SPECIAL MODE IS NORMAL
CHURCHILL 66 2 FLIGHT S BY S=C PENETRATING
NORM ST ELAPSED TIME = 12 MINUTES 43 38/60 SECONDS

Figure A-5

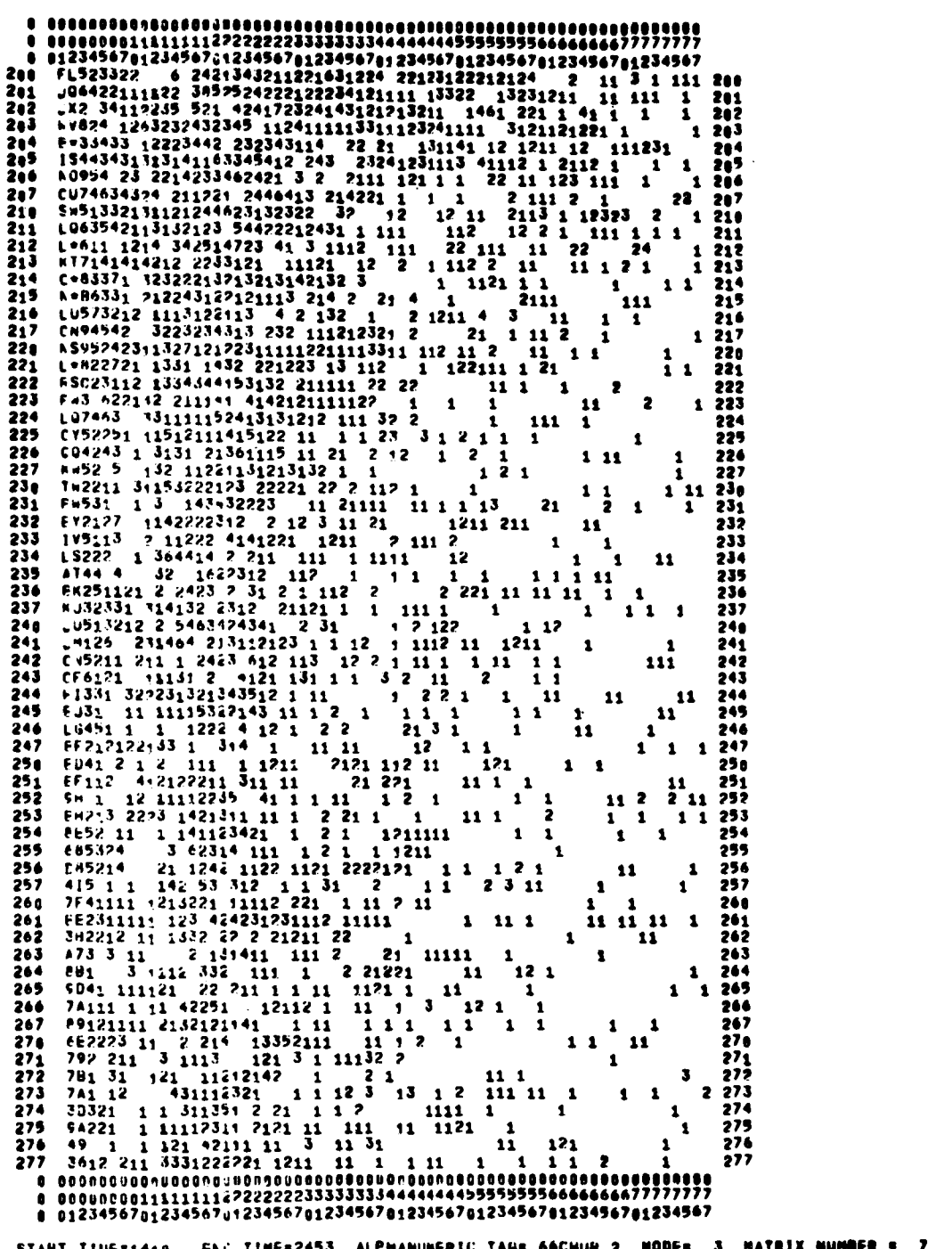
LINEAR ALPHAMERIC OUTPUTIMAX= 38
START TIME=1410 END TIME=2453 ALPHANUMERIC TAG= 66CHUR 2 MODE= 3 MATRIX NUMBER = 7
PENETRATION BIT WAS NOT PENT OUTPUT IS WITH A=X, B=Y SPECIAL MODE IS NORMAL
CHURCHILL 66 2 FLIGHT S BY S-C NOT PENETRATING
NORM ST ELAPSED TIME = 12 MINUTES 43 38/60 SECONDS

Figure A-6

```
LINEAR ALPHAMERIC OUTPUTIMAX=      25

  0 0000000000000000000000000000000000000000000000000000000000000000
  0 0000000011111111222222223333333344444444555555556666666677777777
  0 0123456701234567012345670123456701234567012345670123456701234567
200   31  1    53131HF5EAMECEDPCA9A544D3775655461122  2113 21 1 1141 200
201  11113    1 3453AER9FDDJJKAR9DA49A74357274455312 111214  2311  11 201
202  1  1        12316FA8AGKGAH98CC6435357613744124312 22342322 124 22 202
203   211  ? 1214465CAHIIFDDHA9D6H889A785231434333 5 22144211 13 3 1 203
204   1  1    1 26557C5HK9IDCEIDE8G9A4533555453415212 22  11  1131113 204
205  43  11    114455506BJPI9EADAJ85896884547431132252412142222   1112  205
206  11  1 131 22363C5AFGDEFIA79795865342 2 3 1 241252 1    341 1  21 206
207  3 2  1 1    12476HHLCKFMDIDD8C826C52613141312 11 2 23311 11    13 207
210  1312      14 2545FA6HHFKHIDFCC7985A6325423  1224 123  12111 11  1 210
211  111         11379CCDFLABEF9CC7677553223423312 1351 1111 221112  13 211
212  12 11 1 1 3245796DAH7AJJAB67F49742435262 45   3511 4      1121311 212
213  1 2 1211 12 1468AGGGBJ6A6AC48353641      2132 2 122  1111  2212  213
214  131 2    12 3214C7HEFFG9B99A7C3656754312  1 1 2 1  122 1 211 1   214
215  2221    1  2 1874P7CBHAC8RIF85738213  22333111 221    3  ?  2 2   215
216  32   1      1124455DEA9HD8GRH44457541331142 3121   211        1 1   216
217  1131     1 2 2546A3CBCEFECHR7A7A667A233  2 2  12 341 3   1   1     217
220  14 1     121 32268RCAGGFDDGA64A73664254  2  1 41  4 2 1 1  311     220
221  121 21   1 4254797ADAFEE64AD977557222113212 1       1        11 1  221
222  12 12 1 121232 7597ACDFECRR665446451212 11  21 3111    1221 11     222
223   11     11 23246E86CAHDGA6996955C1213233 1 2 1    1 2  21 1  1  11 223
224  23    1 11   344587EF6G9JAACB78A2624 322  211 1      231 111 1  2  224
225   11   11   1222 25544F75DBC8R64338333 22114 1111    1112 21   11   225
226  312    1 1 14 44377RRABRHHCR6673792245 22 1   2     1 22 1   1  2  226
227  11  1  11   113975B986EBCICE4F96133 31121211    1     1    1 1   1 227
230   21  1111 34 14235BDE79AGB957556352 21 ?  341  1    11 11111   1  230
231  311 ? 1 12  264454489EBIAC83667252332 32 1 32 1 1111212 11    21 231
232  1 1  2 1 14 1118P59DCDCAAC9593634845 31 3  31   11 11      111     232
233  22 2         1123243AB6999RDC5A4267232 233 21111 1    13 1    2 1  233
234  12                1234B5C8DAEICA5694931441312111111 1    11 1  1      234
235   2  1  1 2  13357346BAA58949R64434321121 1121       1221 1  112    235
236   211  1  1 1111495767AF7KA7444515644 12111  12  2  1 1  1  1 1  236
237  111  1  1      33437R65677887555567 3324512111112     11      121 1 237
240   21 1      11 3111 95CBA99AAA655833333242   21  11 14        1 1   240
241  1211 121 122 1213247A4FAC5E364723313 1232 12 122  12      12 1 1 241
242   1   11 11 2  3463567AAB7R668A7571343121   2311   112             242
243   2 1  1 111 13 27558799AB79755A8141 21211 1 1  313 2      1111     243
244  14      1    111146671167 3ABAC4448476 224343 311 11      111 1     244
245  2  11       11     333156A62575B9363426131111 1 1   1 1 1 1  11  121 245
246   11 111     1 21117567767784865A565433217312121311111  1 111      11 246
247  14 11        21 1 1123359DH87738765121 2 15221 1 1   1  12 2  1 1  247
250  22  1  1     1 2 2124938575842757874314432223 2   1 1 1111 1   2  250
251  351    1      12   312187436553546433 12333 22 12211 1 21 12 11 1 1 251
252  13111              1371 37657989745643914 34216  2111   1  112 211   252
253  2131 1111 1 2142 4325437456A66334322752116 112111  121        32  253
254  14           2   1 312126688674A34235322323 1111121  1      1 11    254
255   2  1        1   2112225 64C77769155 43343111 212   3     212 1  1  255
256  21     1  1112 11121 47448471 A3864 323 2121511 1213        1111     256
257  21111   1    1 3 121346424 33A5775 254432 211 1111111   2   1    1 257
260  331  1 1  1 11  41663134345A754524574 33222321  11     1 22 1 1  1 260
261   1     2     1121  14667732 3533564234624 12  4122   22 1   1 11   261
262  131     1  1 211   43323677845574R7465321  3 13      211 2   11     262
263  131 1 1   2  1    1111 35367A6484354322  32223 23  3 4 1           1 263
264  213    ? 11 1  1 1212432 23A47295642 05232321  211  22321 1      1  264
265  1 1    1     13 1 3 1112 45548774 17253742 3262 1233111 13   1 21      265
266  121  11  1121     113242335 3R344583624 412621 2 121  2     21 41    266
267  151   1   11     2 3252A446 4651127391533 23  1112  111  1 2  11 1 267
270  1 2111   1  1 12 11115 41453253824533482 31361112 2  31 1 12 1      270
271  23111           1 11 3213111574652 54A3133 12 11 1 2 1 221 2 11 2  1   271
272  33     2 1    1  11 2136333 32 44146 6541323 2241311 211112  112    1 272
273  172  11 11113  1  21633462 65214 1A522315 2121211 121    1111  2    273
274   1         1    1 1    25 52213363444422 3514111  11 21 111      1 1  274
275   221    1        2    1 23 1 21116113112331 11 11  2  111    2 11 1  275
276  12                     1 1  21      1 2 21       1        1         1   276
277                         1                                              277
  0 0000000000000000000000000000000000000000000000000000000000000000
  0 0000000011111111222222223333333344444444555555556666666677777777
  0 0123456701234567012345670123456701234567012345670123456701234567

START TIME=1410   END TIME=2453  ALPHANUMERIC TAG= 66CHUR 2  MODE=  3  MATRIX NUMBER =  7
PENETRATION BIT WAS PENETRAT  OUTPUT IS WITH A=Z, B=Y  SPECIAL MODE IS NORMAL

 CHURCHILL 66 2 FLIGHT  S PRIME BY S+C  PENETRATING
NORM ST ELAPSED TIME =     13 MINUTES  4 29/60 SECONDS
```

Figure A-7

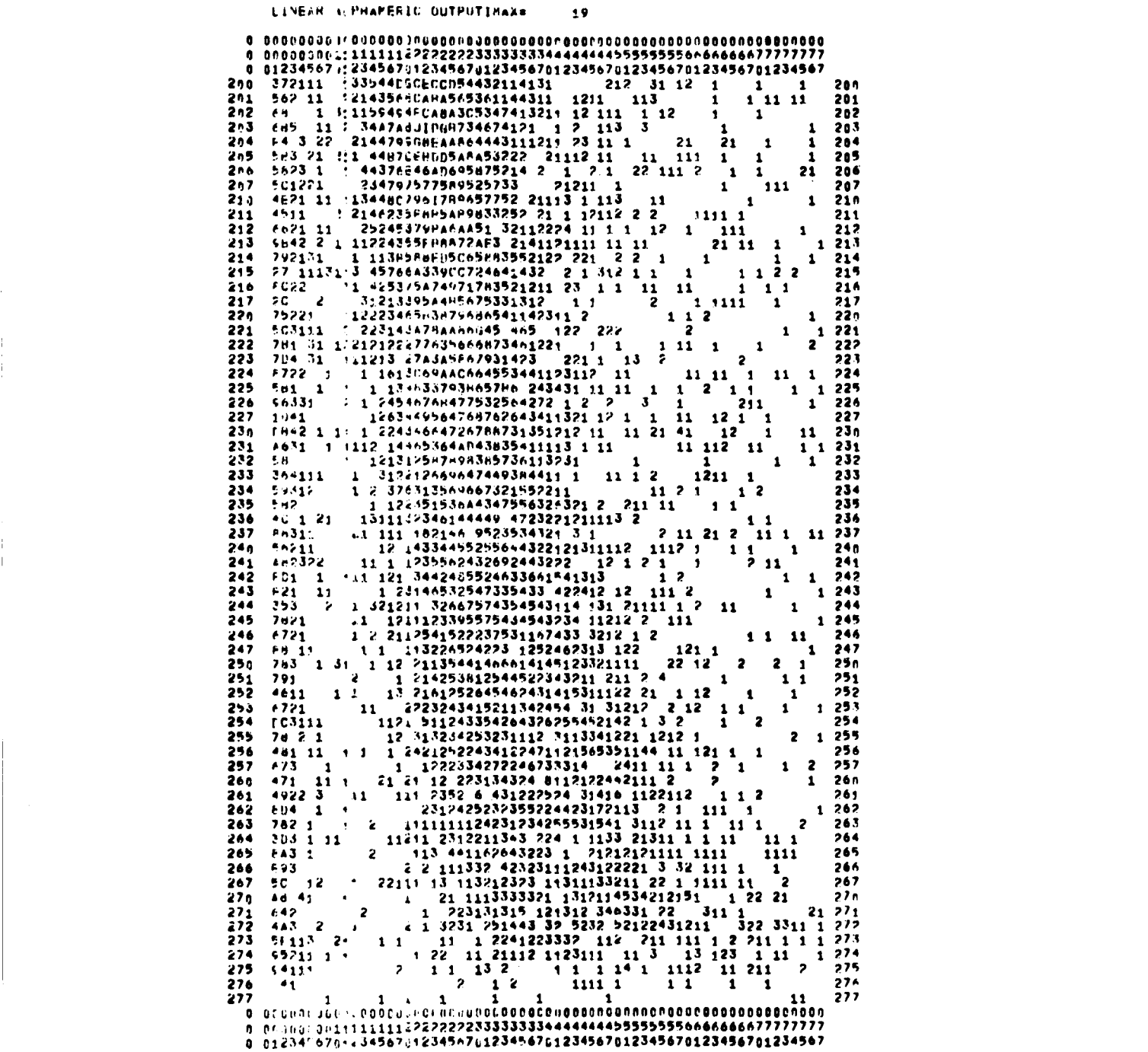
LINEAR & PHAMERIC OUTPUTIMax= 19
START TIME=3431 END TIME=2453 ALPHANUMERIC TAG= 66CHUR 2 MODE= 3 MATRIX NUMBER = 7
PENETRATION BIT WAS NOT PENT OUTPUT IS WITH A=Z, B=Y SPECIAL MODE IS NORMAL
CHURCHILL 66 2 FLIGHT S PRIME BY S&C NON PENETRATION

Figure A-8

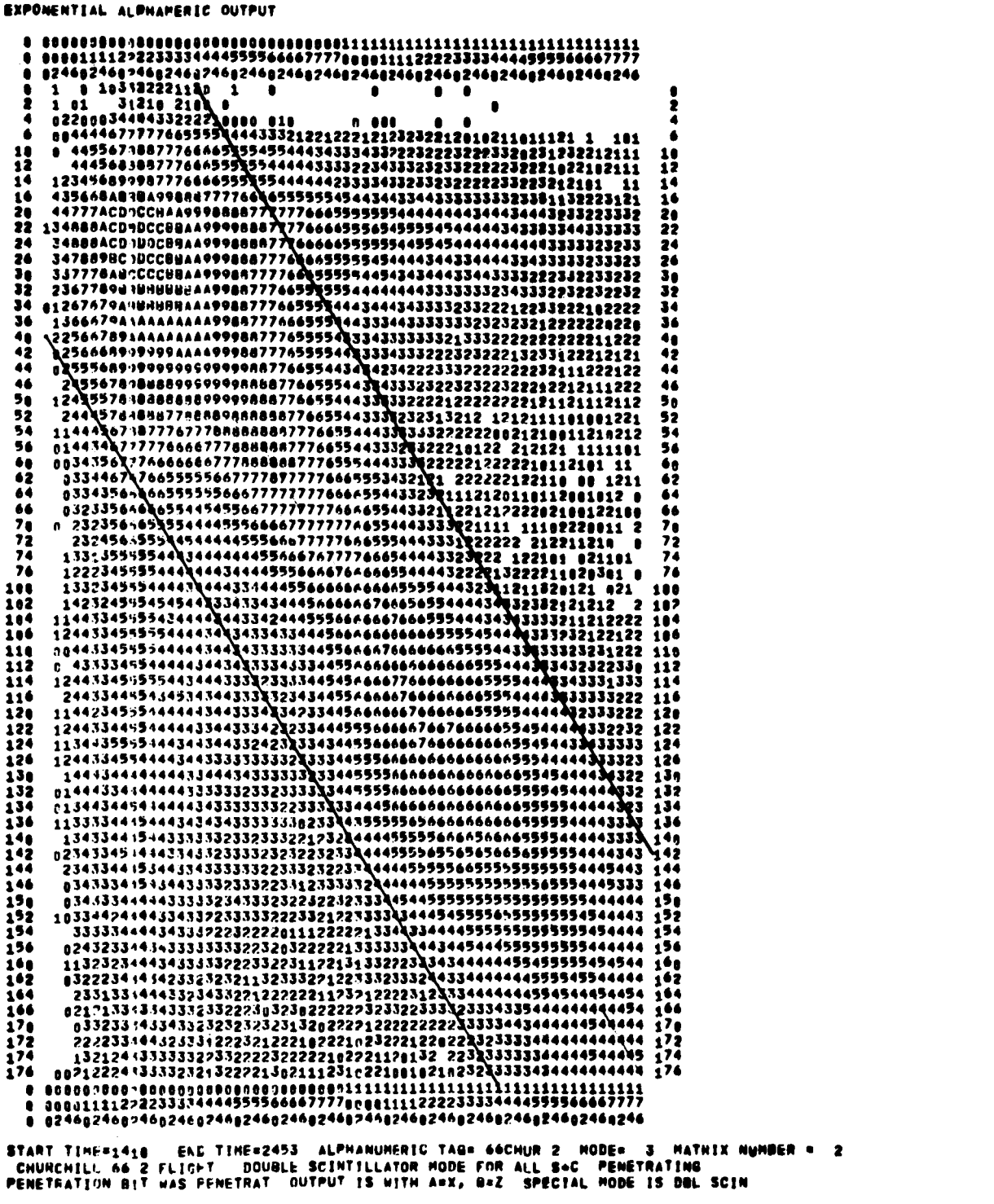
EXPONENTIAL ALPHAMERIC OUTPUT
START TIME=1418 END TIME=2453 ALPHANUMERIC TAG= 66CHUR 2 NODE= 3 MATRIX NUMBER = 2
CHURCHILL 66 2 FLIGHT DOUBLE SCINTILLATOR MODE FOR ALL S=C PENETRATING
PENETRATION BIT WAS PENETRAT OUTPUT IS WITH A=X, B=Z SPECIAL MODE IS DBL SCIN

Figure A-9

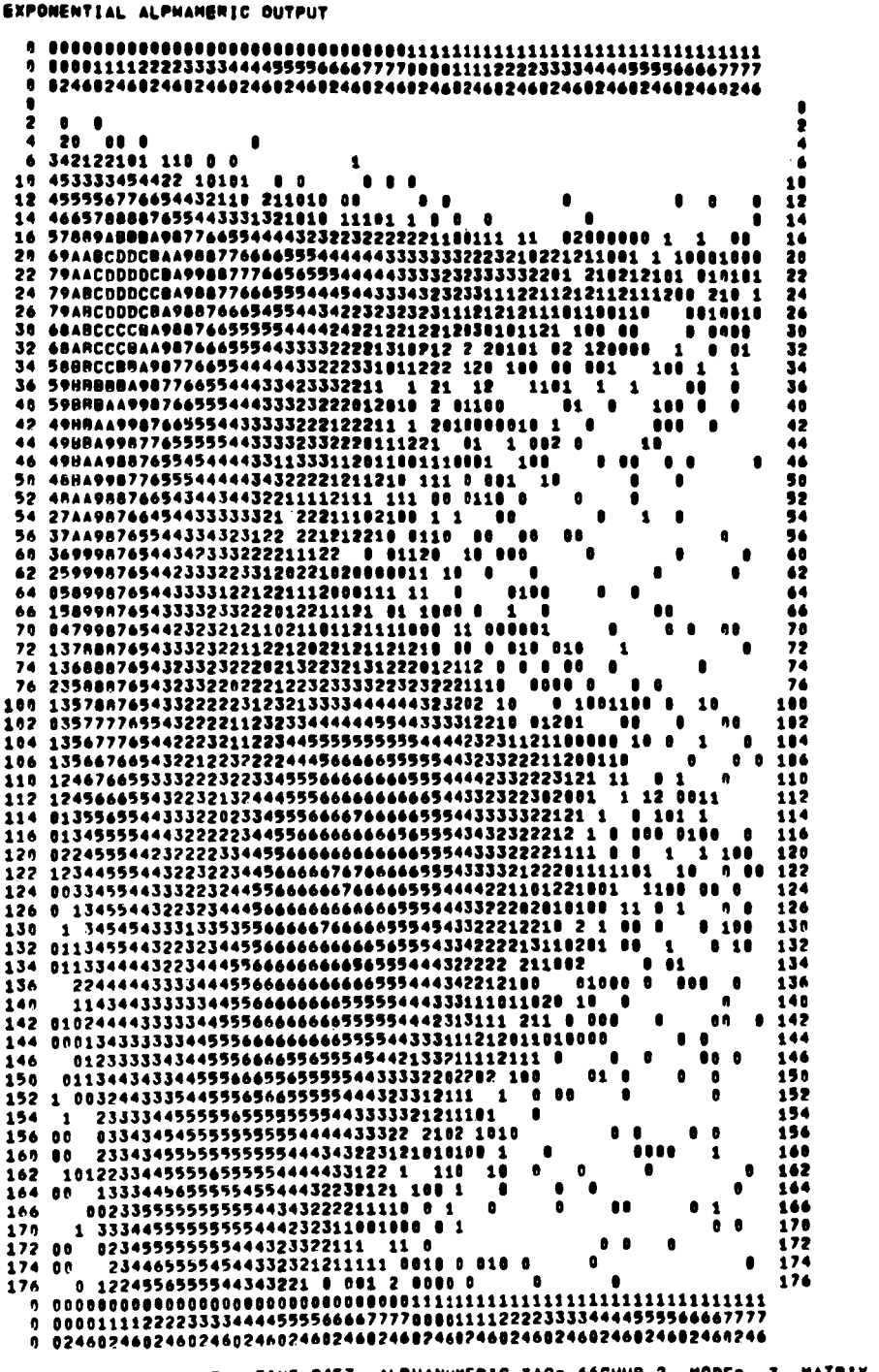
EXPONENTIAL ALPHAMERIC OUTPUT
START TIME=1410 END TIME=2453 ALPHANUMERIC TAG= 66CHUR 2 MODE= 3 MATRIX NUMBER = 3
CHUR 66-2 PENETRATING SELECT IF ABS(S TOP - S MID) .LT.32.AND.LT 0.3*SUM
PENETRATION BIT WAS PENETRAT OUTPUT IS WITH A=X, B=Y SPECIAL MODE IS SELECTED

Figure A-10

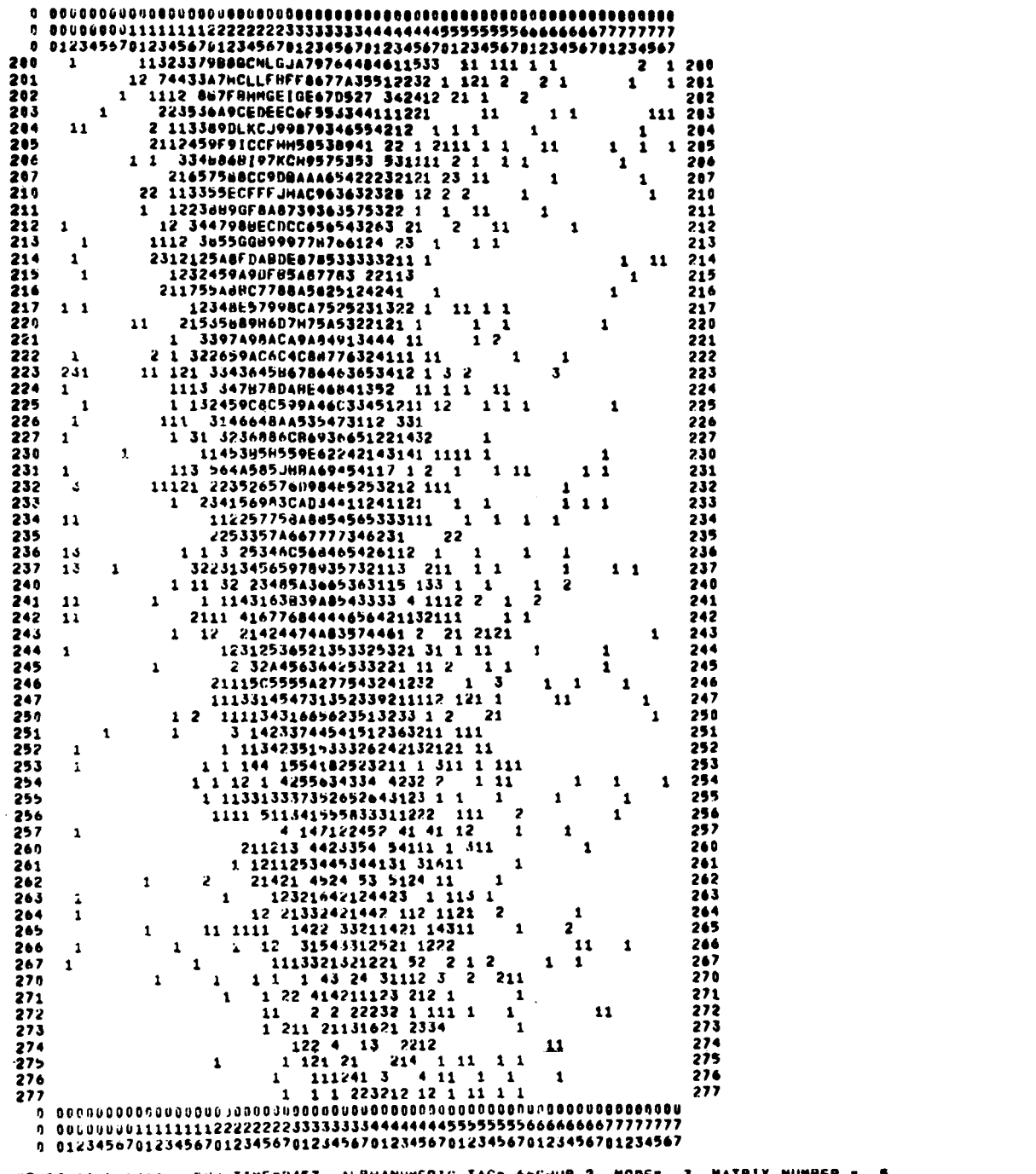
LINEAR ALPHAMERIC OUTPUT(MAX= 23
START TIME=1410 END TIME=2453 ALPHANUMERIC TAG= 66CHUR 2 MODE= 3 MATRIX NUMBER = 5
PENETRATION HIT WAS PENETRAT OUTPUT IS WITH A=X, H=Y SPECIAL MODE IS SELECTED
CHUR 66-2 PENETRATING SELECT IF ABS(S TOP - S MID) .LT.32,AND,LT 8,3*SUM
NORM SI ELAPSED TIME = 11 MINUTES 2 16/60 SECONDS

Figure A-11

DECOUPLING MATRIX

1.000000	.950000	.870000	.690000	.420000	.000000	0	0	0	0
.920000	1.000000	.930000	.810000	.560000	.100000	0	0	0	0
.800000	.900000	1.000000	.910000	.720000	.340000	.020000	.130000	0	0
.590000	.710000	.860000	1.000000	.800000	.570000	.170000	.330000	.530000	0
.320000	.450000	.620000	.820000	1.000000	.830000	.440000	.620000	.790000	.930000
.050000	.120000	.230000	.440000	.700000	1.000000	.810000	.900000	.900000	.850000
0	0	.010000	.110000	.310000	.600000	1.000000	.900000	.710000	.400000
0	.010000	.000000	.220000	.400000	.040000	.940000	1.000000	.860000	.640000
.040000	.100000	.210000	.410000	.600000	.900000	.850000	.930000	1.000000	.030000
0	0	.450000	.730000	.090000	.910000	.630000	.700000	.900000	1.000000

RESOLUTION MATRIX

.471000	.330300	.173500	.061000	.012700	.000600	0	0	0	0
.157400	.167600	.136700	.075500	.022600	.002900	0	0	0	0
.161700	.209000	.230600	.101200	.000200	.015500	.001100	0	0	0
.092000	.139700	.205000	.239200	.160000	.054900	.004600	0	0	0
.058300	.087100	.154200	.254600	.299700	.109300	.034500	.001200	0	0
.032000	.030300	.070300	.130900	.269300	.355300	.176600	.018000	.000200	0
.071900	.015900	.024800	.044200	.125100	.306700	.475300	.204900	.021100	0
.004000	.003300	.004100	.004700	.070900	.060900	.263900	.494200	.229600	.022700
0	0	0	0	.001400	.005000	.041900	.244300	.476400	.202900
0	0	0	0	0	0	.002000	.037400	.296500	.523400

DECOUPLED MATRIX

.471000	.321305	.150945	.042642	.005334	.000040	0	0	0	0
.144000	.167600	.127131	.061155	.012656	.000922	0	0	0	0
.129360	.100820	.230600	.164092	.057744	.005270	.000029	0	0	0
.054752	.099107	.176900	.239200	.147040	.031293	.000789	0	0	0
.010656	.039195	.095604	.200772	.299700	.157119	.015100	.000744	0	0
.001640	.004596	.016169	.061116	.100510	.355300	.143044	.016020	.000196	0
0	0	.000240	.004062	.030701	.200556	.475300	.102361	.014901	0
0	.000033	.000320	.001034	.010032	.057076	.240064	.494200	.197456	.014520
0	0	0	0	.000952	.005604	.035615	.227199	.470400	.160407
0	0	0	0	0	0	.001260	.029172	.230050	.523400

INVERTED DECOUPLED MATRIX

INVERTED TEN BY TEN

6.456022	-21.404364	9.061420	-1.016527	-.141370	.141307	-.042045	.013209	-.004016	.001101
-7.756029	45.660608	-26.495712	0.934240	-1.106603	.010940	.019009	-.007595	.002039	-.000704
3.169430	-33.646209	33.544106	-19.221619	5.062016	-1.125301	.242071	-.072260	.025035	-.006307
-.625196	12.637000	-20.004616	22.330366	-9.384332	2.035062	-.694910	.212712	-.070553	.019727
.024043	-2.942520	6.973302	-12.512530	10.977453	-4.503011	1.212017	-.379124	.137136	-.033600
.073005	.462755	-1.634535	3.000435	-5.043690	5.719017	-1.009117	.611499	-.223677	.054996
-.007062	-.094730	.300900	-1.060709	1.500922	-2.440997	3.519947	-1.470113	.571350	-.149066
.000333	.053933	-.143659	.334335	-.477045	.747592	-1.051704	3.302097	-1.520973	.390619
.000113	-.020493	.050357	-.114160	.165007	-.260602	.710370	-1.699907	3.267790	-1.004247
-.000049	.006261	-.015140	.034290	-.049970	.079204	-.222110	.565002	-1.357449	2.331643

Figure A-12

REFERENCES

Axford, W.I., 1965, Planetary and Space Science, 13, 115.

Badhwar, G.D., Deney, C.L., Dennis, B.R., and Kaplon, M.F., 1967 a, to be published in Nuclear Instruments and Methods.

Badhwar, G.D., Deney, C.L., Dennis, B.R., and Kaplon, M.F., 1967 b, to be published in the Proceedings of the 10th International Conference on Cosmic Rays.

Balasubrahmanyan, V.K., Boldt, E., and Palmeira, R.A.R., 1967, J. Geophys. Res., 72, 27.

Balasubrahmanyan, V.K., Hagge, D.E., Ludwig, G.H., and McDonald, F.B., 1966, J. Geophys. Res., 71, 1771.

Balasubrahmanyan, V.K., and McDonald, F.B., 1964, J. Geophys. Res., 69, 3289.

Birks, J.B., 1951, Proc. Phys.Soc., (London), 64A, 874.

Coleman, P.J., 1966, Journal of Geophysical Research, 71, 5509.

Dorman, L.I., 1963, Progress in Elementary Particles and Cosmic Ray Physics, VII, North Holland, Amsterdam.

Durgaprasad, N., Fichtel, C.E., and Guss, D.E., 1967, J. Geophys. Res., 72, 2765.

Elliot, H., Hynds, R.J., Quenby, J.J., and Wenk, G.J., 1960, Proceedings of the 6th International Conference on Cosmic Rays, Moscow.

Emhert, A., 1960, Proceedings of the 6th International Conference on Cosmic Rays, Moscow.

Fan, C.Y., Gloeckler, G., and Simpson, J.A., 1966, Phys. Rev. Lett., 17, 329.

Freier, P.S., and Waddington, C.J., 1965, Proceedings of the 9th International Conference on Cosmic Rays, London, 1, 176.

Gooding, T.J., and Eisberg,R.M., 1957, Physical Review, 105, 357.

Hofmann, D., and Winckler, J.R., 1967, Planet, Space Sci., 15, 715.

Jenkins, R.W., 1966, Ph.D. Thesis, University of Alberta, Calgary.

Jokipii, J.R., 1966, Astrophys. J., 146, 480.

Jokipii, J.R., 1967, to be published in the Proceedings of the 10th International Conference on Cosmic Rays, Calgary.

Landau, L., 1944, Journal of Physics, 8, 201.

Lietti, B., and Quenby, J.J., 1967, to be published in the Proceedings of the 10th International Conference on Cosmic Rays, Calgary.

Lockwood, J.A., and Webber, W.R., 1967, J. Geophys. Res., 72, 3395.

Lund, N., and Risbo, T., 1965, Technical Report CC-1, Cosmic Ray Group, The Technical University of Denmark, Lyngby, Denmark.

McDonald, F.B., and Ludwig, G.H., 1964, Phys. Rev. Lett., 13, 783.

Mead, J.B., and Martin, J.P., 1965, Nuclear Instruments and Methods, 36, 13.

Nagashima, K., Duggal, S.P., and Pomerantz, M.A., 1966, Planetary and Space Science, 14, 177.

Ness, N.F., Scerce, C.S., and Cantarans, S., 1966 a, Journal of Geophysical Research, 71, 3305.

Ness, N.F., Scerce, C.S., Seek, J.B., and Wilcox, J.M., 1966 a, Space Research, 6.

O'Gallagher, J.J., and Simpson, J.A., 1967, Astrophysical Journal, 147, 819.

Ormes, J.F., 1965, M.S. Thesis, University of Minnesota.

Ormes, J.F., and Webber, W.R., 1964, Phys. Rev. Lett., 13, 106.

Ormes, J.F., and Webber, W.R., 1965, Proceedings of the 9th International Conference on Cosmic Rays, London, 1, 349.

Ormes, J.F., von Rosenvinge, T., and Webber, W.R., 1967, Astrophys. J.,

Parker, E.N., 1956,Phys. Rev., 103, 1518.

Roeloff, E.C., 1966, Ph.D. Thesis, University of California, Berkeley.

Sawyer, D., Ormes, J.F., Webber, W.R., and Bingham, G., 1967, to be published in the Proceedings of the 10th International Conference on Cosmic Rays, Calgary.

Shea, M.A., and Smart, D.F., 1967, Journal of Geophysical Research, 72, 2021.

Silberberg, R., 1966, Phys. Rev., 148, 1247.

Skadron, G., 1967, Technical Report 678, University of Maryland.

Sternheimer, R.M., 1953, Physical Review, 91, 256.

Sternheimer, R.M., 1956, Physical Review, 103, 511.

Sternheimer, R.M., 1960, Physical Review, 117, 485.

Subrahmanyan, P., and Ammiraju, P., 1965, Nuclear Instruments and Methods, 33, 87.

Symon, K.R., 1948, Ph.D. Thesis, Harvard University.

Teegarden, B.J., 1967, Ph.D. Thesis, University of Maryland.

Webber, W.R., 1967, to be published in the Proceedings of the 10th International Conference on Cosmic Rays, Calgary.

Webber, W.R., and Ormes J.F., 1963 a, Proceedings of the 8th International Conference on Cosmic Rays, Jaipur, 3,3.

Webber, W.R., and Ormes, J.F., 1963 b, Proceedings of the 8th International Conference on Cosmic Rays, Jaipur, 3, 69.

Webber, W.R., and Ormes, J.F., 1967 a, J. Geophys. Res., 72, 3387.

Webber, W.R., and Ormes, J.F., 1967 b, to be published in the J. Geophys. Res.

Webber, W.R., Ormes, J.F., and von Rosenvinge, T., 1965, Proceedings of the 9th International Conference on Cosmic Rays, London, 1, 407.

Verma, S.D., 1966, Ph.D. Thesis, University of Chicago.